Characterization and Performance Assessment of SiO_2-KCl-Xanthan Nanocomposite as a Novel nano-Asphaltene Precipitation Inhibitor under Laboratory Conditions

By

Kemelkhan Kaliolla

Thesis submitted to the School of Mining and Geosciences of Nazarbayev University

in Partial Fulfillment of the Requirements for the Degree of

Master of Science in Petroleum Engineering

Nazarbayev University

April 2024

ORIGINALITY STATEMENT

I, Kemelkhan Kaliolla, hereby declare that this submission is my own work and to the best of my knowledge it contains no materials previously published or written by another person, or substantial proportions of material which have been accepted for the award of any other degree or diploma at Nazarbayev University or any other educational institution, except where due acknowledgement is made in the thesis.

Any contribution made to the research by others, with whom I have worked at NU or elsewhere is explicitly acknowledged in the thesis.

I also declare that the intellectual content of this thesis is the product of my own work, except to the extent that assistance from others in the project's design and conception or in style, presentation and linguistic expression is acknowledged.

Signed on **15.04.24**

_____

NOMENCLATURE

Acronyms and Abbreviations

AOP	Asphaltene onset point
APE	Asphaltene phase envelope
BET	Brunauer-Emmett-Teller
EOR	Enhanced oil recovery
FTIR	Fourier-transform infrared spectroscopy
IUPAC	International Union of Pure and Applied Chemistry
NC	Nanocomposite
n-heptane	Normal heptane
NP	Nanoparticle
SARA	Saturates, aromatics, resins, asphaltenes
SEM	Scanning electron microscope
TGA	Thermogravimetric analysis
UV	Ultraviolet-visible
XRD	X-ray diffraction

Symbols

A	Surface area of NC, m^2/g
A_d	Asphaltene absorbance after dilution
A_i	Initial absorbance of asphaltene
C_e	Equilibrium asphaltene concentration, mg/L
C_0	Initial asphaltene concentration, mg/L
C_{NP}	Nanoparticle concentration, g/L

$\frac{m_{NP}}{C_0}$	NP mass per Initial Asphaltene Concentration, $\frac{\text{g}}{\text{mg/L}}$
C_d	Concentration of asphaltene after dilution
K_F	Freundlich constant
K_L	Langmuir constant
M	Mass of asphaltene, mg
m	Mass of NC, g
m_{ads}	Mass of adsorbed asphaltene, g
$m_{TGA(ads+NP)}$	Mass of adsorbed asphaltene and NP from TGA, g
$m_{TGA(NP)}$	Final mass of NP, g
Q_e	Equilibrium asphaltene amount per surface area, c
q_{eq}	Equilibrium asphaltene concentration, mg/g
Q_m	Maximum amount of adsorbed asphaltene per surface area
s	the equilibrium adsorbate uptake per surface area of the adsorbent (mg/m^2)
V_1	Volume of synthetic oil, ml
V_2	Volume of toluene, ml

Greek Letters

ε	Molar absorption coefficient, $M^{-1}cm^{-1}$
λ	Spectrophotometry wavelength, nm

Metric Conversion Factors

1 ppm	1 mg/L
1 mD	9.869×10^{-16} m^2
1 bbl	0.159 m^3
1 nm	10^{-9} m

ABSTRACT

In this experimental research work, efficiency of SiO_2-KCl-Xanthan nanocomposite (NC) as a nano-inhibitor for adsorption and removal of asphaltene from a synthetic crude oil medium was investigated. The NC has been used as an EOR and smart drilling fluid agent with impressive results. This was the motivation behind this research work. The first phase of the research involved extraction of asphaltene from a West Kazakhstani heavy crude oil and characterization of both asphaltene and the NC. Different state of the art analytical techniques including scanning electron microscopy (SEM), Fourier-transform infrared spectroscopy (FTIR), Brunauer-Emmett-Teller or BET, X-ray diffraction (XRD), and thermogravimetric or TGA were used for NC. This was to ensure authenticity and functionality of the NC. The NC has a spherical structure with particle sizes ranging from 30 to 300 nm determined using SEM analysis. The crystallite size was calculated 41 nm using the XRD data. The surface area of the NC was determined 31.95 m^2/g using the BET method. TGA analysis showed that the NC did not experience any significant mass loss for a typical reservoir temperature (80°C) and it is thermally stable for oilfield applications. Based on the FTIR spectra, presence of organic functional groups of phytochemicals on the NC was identified indicting successful synthesis of the NC. The last stage was to assess the efficiency of the nano-inhibitor by determining the Asphaltene Onset Point (AOP) using UV-vis spectroscopy technique and asphaltene adsorption kinetics isotherm modeling using the supernatant obtained from TGA analysis. TGA analysis confirmed that oxidation of virgin asphaltene started at around 400 to 450℃. While, oxidation of 5,000 ppm sample with NC started at around 280℃. The NC has catalyzed oxidation of the asphaltene. Adsorption kinetics isotherm modeling was done using the Langmuir (R^2 = 0.98) and Freundlich (R^2 = 0.82) isotherm models. The experimental data matched well both models, which suggests monolayer and multilayer adsorption behavior for adsorption of asphaltene onto the surface of the NC. A maximum adsorption capacity of 1.33 mg/m^2 was obtained for the NC. The novel nano-inhibitor shifted the AOP by 5% and the optimum concentration of NC was determined 0.3 wt%. Overall, the NC showed promising inhibitory performance under laboratory conditions.

***Keywords*:** Asphaltene precipitation inhibition, nano-inhibitors SiO_2-KCl-Xanthan nanocomposite, adsorption, AOP

ACKNOWLEDGEMENTS

I wish to express my deepest gratitude to all those who have contributed to the completion of my dissertation. Foremost, I am indebted to my supervisor, Dr. Ali Shafiei, for his invaluable guidance, discerning critique, and steadfast encouragement throughout every stage of this study. Additionally, I extend my sincere appreciation to my co-supervisor, Dr. Timur Atabaev, whose mentorship, support, and provision of access to his research laboratory were instrumental in executing the experimental aspects of my research.

I am also thankful to Dr. Rouzbeh G. Moghanloo (University of Oklahoma) and Dr. Chang Hong Gao for acting as my thesis examiners. Their constructive feedback significantly enhanced the quality of this dissertation.

This work was conducted as part of the Collaborative Research Proposal Faculty grant project (OPCRP2020015), titled: “A comprehensive study on asphaltene characterization and screening asphaltene deposition inhibitors for Kazakhstan crude oils.” I am grateful to Nazarbayev University for the financial support extended through this grant.

I extend my appreciation to the School of Mining and Geosciences faculty and staff and at Nazarbayev University for providing an exceptional academic environment, access to resources, and encouragement throughout my journey. Special thanks are also due to research team members Kamilya Arstanova and Yuliya Ten for their insightful comments, ideas, and motivational support.

To my family and friends, I owe an immeasurable debt of gratitude for their unwavering love, encouragement, and inspiration throughout my academic pursuits. Their unwavering belief in me has been a constant source of courage and motivation on this journey.

LIST OF FIGURES

LIST OF TABLES

1. INTRODUCTION

In this chapter, first background information on importance of the petroleum industry as the major source of primary energy worldwide is provided followed by definition of asphaltene and the issues caused by asphaltene deposition in the oil industry with emphasis on asphaltene deposition in Kazakhstani oil reservoirs. A brief review of asphaltene precipitation and deposition process and methods used to mitigate the adverse effects of asphaltene deposition is also provided. Then, the problem statement along with the designed research methodology used to execute the proposed research work, the research objectives, and structure of the dissertation are described.

1.1 Background

Contribution of the oil and gas industry to the global energy market has grown by 1.3% after the global pandemic according to World Energy & Climate Statistics – Yearbook 2022. Forecasts for the next 30 years also show a significant demand for energy. Petroleum is the main source of global primary energy along with coal in major developing economies (i.e., India and China) (Enerdata, 2022).

Asphaltene precipitation and deposition is a significant and worldwide problem during oil production and other processes related to transportation and storage of crude oil (Adebiyi, 2021). During the production and the natural decline in pressure, the crude oil starts to expand due to swelling effect. Asphaltene particles dissolve in the crude oil because of this swelling and asphaltene particles start to aggregate and precipitate out of the crude oil phase at asphaltene onset pressure (AOP) and form a new phase. This can lead to deposition of asphaltene in the reservoir (i.e., porous media), tubing, and other production facilities. Adsorption of asphaltene onto surface of reservoir rocks can cause reduction in permeability (i.e., formation damage) due to clogging of pores (Mohammed et al., 2021). Deposition of asphaltene has the potential to change reservoir rock's wettability, to reduce permeability inside reservoirs, and to cause formations damage (Tavakkoli et al., 2017).

Crude oil is a mixture of hydrocarbons with various components of organic and metallic basis. Asphaltene as one of the constituents of crude oil is known for its complex molecular structure, high molecular weight, and composition and its tendency for aggregation and accumulation. Asphaltene is soluble in aromatic solvents and insoluble in light hydrocarbons such

as pentane or hexane (Alimohammadi et al. 2019). Depletion of reservoir pressure leads to aggregation and precipitation of asphaltene. Asphaltene deposition is mainly causes due to drop in pressure. PT diagram of asphaltenic fluids is presented in Figure 1-1. As one can see from the Figure 1-1, with reduction in reservoir pressure below saturation pressure (P_b) which is known as the upper boundary of asphaltene precipitation, the asphaltene particles start to aggregate and eventually precipitate and form a deposit in the pore space or on the wall of pipes, tubing, and or surface facilities. The pressure level below P_b where the liquid, gas, and asphaltene phases exists marks the lower boundary of asphaltene stability on the PT diagram (Soleymanzadeh et al. 2019). Based on saturate, aromatic, resin and asphaltene (SARA) analysis and some microscopic scale investigations, asphaltene particles are usually covered with a layer of resin in crude oils. Depressurization leads to a rupture in the resin layer, after which the aggregation of particles begins and they become stabilized.

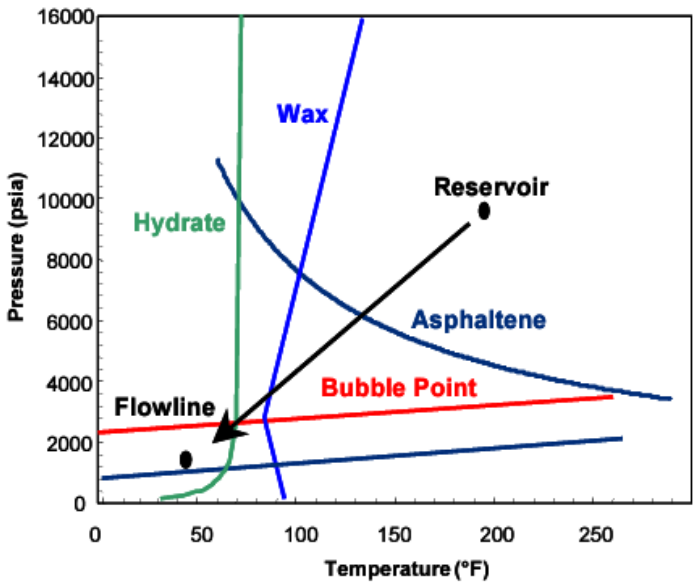

Figure 1-1. Phase diagram of a black oil obtained from the Gulf of Mexico (Ratulowski et al. 2004).

1.2 Relevance to the Industry

Problems caused by asphaltene deposition is widespread in Kazakhstani oilfields. Several oilfields especially in the western part of the country suffer from adverse effects of asphaltene deposition. In addition, it impacts crude oil production, transportation, and storage (Soroush et al., 2021). The elevated levels of heteroatoms in crude oils can make the asphaltene deposition even worse (Ibrahim and Idem, 2004). Common mitigation measures include controlling the system's temperature, pressure, and solid formation conditions as well as regularly stimulating the well with a mixture of mutual solvent, xylene, and acid (Al-Qasim et al., 2018). The past few decades, research on application of nanotechnology in various sectors in the petroleum industry is being conducted with some field applications. This is because of small size and large surface area of nanoparticles (NPs) giving them extraordinary features. Researches are reported on development and application of nano-inhibitors for efficient adsorption, oxidation, and removal of asphaltene is crucial (Mazloom et al., 2020) (Ngata et al., 2021).

1.3 Statement of Problem

Asphaltene deposition during oil production and gas injection into reservoirs is reported from around the world, including Kazakhstan. This macro-problem during fluid flow is accompanied by numerous micro-problems such as blockage of pores, deposition of asphaltene in wellbore and during transportation through pipelines (Kuzenbayev, 2022). Immediate actions as mitigation measures usually include mechanical and chemical methods. However, these methods have shown to be very costly or less effective over time resulting in continued deposition and greater damage. Nanomaterials can effectively solve the macro-problems starting from the nano level. Earlier investigations on the effects of SiO_2, NiO, and Fe_3O_4 NPs on oil recovery as well as their ability to adsorb asphaltene and stop it from precipitating showed good performance (Kazemzadeh et al., 2015). Additionally, selection of a proper NP/NC with polymer coating to provide control on their functions seems a more attractive idea rather than using individual NPs (Mazloom et al., 2020). Polymer coating onto metal oxide NPs had higher asphaltene adsorption than the uncoated samples (Farooq et al., 2021). The use of this type of functionalized nanocomposites (NC) is more beneficial.

1.4 Research Objectives

Each individual NP has its own properties and capacity for adsorption of asphaltene. However, combination of different NPs and polymer provides a composite nanomaterial, which possesses collective properties of the individual NPs plus the polymer and has enhanced features and properties. This is why such complex functionalized NCs have attracted the attention of researchers. The main objective of this research work was to investigate performance of SiO_2-KCl-Xanthan as a novel asphaltene nano-inhibitor in a synthetic crude oil medium. This exceptional NP has already demonstrated an extraordinary performance as an EOR and smart drilling fluid agent. However, there were prerequisites for conducting this research and achieving the main objective. These include extraction and characterization of asphaltene from a west Kazakhstani crude oil and synthesis and characterization of the SiO_2-KCl-Xanthan. To this end, this research work was designed to fulfill the following goals defined:

- To extract and characterize asphaltene from a west Kazakhstani crude oil. The characterization was done using XPS (chemistry), SEM (surface morphology and particle size) and FTIR (chemistry and functional groups) and elemental analysis (chemistry) to provide a good understanding of chemistry of the asphaltene and its functional groups,
- To synthesis and characterize the SiO_2-KCl-Xanthan NC. Characterization of the NC was carried out using various analytical techniques including SEM (surface morphology and particle size), XRD (crystal size and chemistry), XPS (chemistry), FTIR (chemistry), BET (surface area), and DLS (particle size).
- To assess the performance of the SiO_2-KCl-Xanthan NC as a novel nano-inhibitor for adsorption and inhibition of asphaltene from a synthetic crude oil medium. The performance assessment partly included UV-vis spectroscopy to determine asphaltene onset point (AOP) in absence and presence of the NC. Furthermore, to determine the optimum concentration of NC to achieve the best performance,
- To conduct thermogravimetric analysis (TGA) to assess thermal stability and adsorption kinetics of the asphaltene-NC system and obtain its adsorption kinetics isotherm models. The TGA data was used in addition to investigate oxidation and the possible catalytic effect on the asphaltene-NC system.

1.5 Research Methodology

The proposed research work was conducted in four phases (Figure 1-2) as it follows to actualize the research objectives defined in the previous section:

- Phase 1. Extraction of asphaltene. The asphaltene extraction was conducted according to the IP-143 standard and preparation of synthetic crude oil as the medium for conduction of performance assessment tests.
- Phase 2. Synthesis of the NC according to the methodology previously described in the literature.
- Phase 3. Characterization of the nanocomposite using various analytical techniques: SEM, BET, FTIR, DLS, TGA, and XRD.
- Phase 4. Performance assessment of the novel nano-inhibitor using UV spectroscopy and TGA analysis.

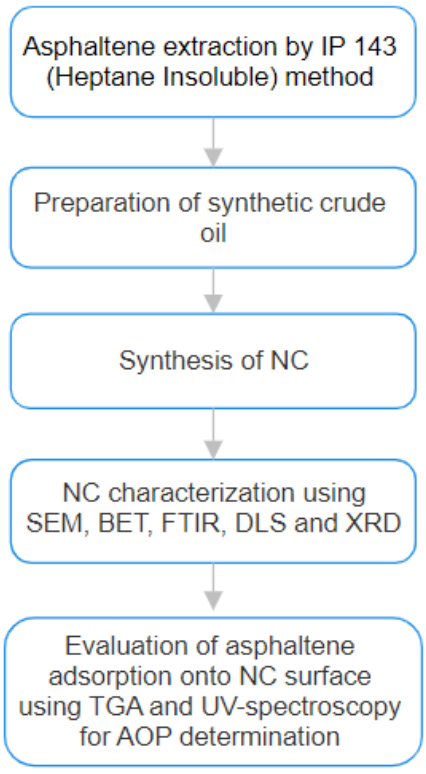

Figure 1-2. Various steps in conducting the research.

1.6 Thesis structure

This dissertation was designed and organized in five chapters. Chapter 1 contains a succinct background information on contribution of the petroleum industry to the global primary energy demand, definition of asphaltene and the flow assurance issues caused by asphaltene deposition in Kazakhstan and worldwide, asphaltene precipitation and deposition process, and asphaltene deposition mitigation measures. The problem statement, research methodology, and objectives are also described. Chapter 2 is the literature review that consists of a critical review of the relevant literature to the core subject of the proposed research including the current state of the art methods used. A number of relevant high-quality research works on asphaltene nano-inhibitors, characterization techniques for asphaltene and nanomaterials, adsorption kinetics of asphaltene onto nanomaterials have been reviewed and analyzed. The materials and experimental methods and equipment used to conduct the proposed research along with step-by-step experimental procedures for each test are described in Chapter 3. The results obtained from various parts of the research work including nanocomposite characterization, asphaltene extraction, and characterization, UV spectroscopy and AOP determination, adsorption kinetics and isotherms, and TGA analysis are presented and discussed in Chapter 4. As summary of major findings and conclusions of the conducted research work along with some recommendations for further future research are provided in Chapter 5.

2 LITERATURE REVIEW

In this chapter, a critical review of the relevant literature to the core subject of the proposed research including the current state of the art methods used is presented. A number of relevant high quality research works on asphaltene nano-inhibitors, characterization techniques for asphaltene and nanomaterials, adsorption kinetics of asphaltene onto nanomaterials. This chapter begin with introducing the asphaltene molecules and their properties, structure, thermodynamic behavior based on the previous works on this topic. Then, the chapter continues with asphaltene deposition causes and impacts of operational parameters and reservoir condition on asphaltene precipitation and deposition. Then, characterization techniques for both asphaltene and nanomaterials are discussed. Metal based NPs as asphaltene inhibitors are described mainly from laboratory and field research works reported from various countries. The mechanisms behind function of nano-inhibitors for asphaltene adsorption and inhibition is also discussed, briefly.

2.1 Asphaltene

2.1.1 Asphaltene definition

Asphaltene is a component of crude oil that proposed for the first time by J.B. Boussingault (Akbarzadeh et al. 2007). Asphaltene is a complex high molecular weight organic compound, insoluble in aliphatic solvents and soluble in aromatic solvents. The molecular structure of asphaltene is the most significant factor controlling its precipitation (Hassanzadeh and Abdouss, 2023). Their aromatic composition also contributes to their dark color.

2.1.2 Asphaltene precipitation and deposition problem

Deposition of asphaltene is an important and widespread problem in the oil industry leading to significant economic losses and operational difficulties. Deposition issues in wells and reservoirs worldwide may result because of asphaltenes can adsorb onto rock surfaces and alter their properties (Marczewski and Szymula, 2002). Disposition of asphaltenes in oil production facilities can result in equipment failure, reduced oil production rates, and pipe blockages. It is crucial to understand the behavior of asphaltenes and create effective techniques to manage the deposition (Speight, 2006). Finding more cost-effective mitigation measures is crucial because cyclic workovers are expensive (Limanowka et al., 1999).

Asphaltenes precipitate when the crude oil expands and dissolves them once enters the well and encounters a temperature and pressure drop. Pressure drop leads to asphaltene coming out of the oil and forming a new phase. Usually, asphaltene settles when the reservoir is fully saturated. Point where asphaltene begins to clump together is called AOP (Sullivan et al., 2020). "Onset point" refers to the lowest amount of the agent needed to separate asphaltene from crude oil. The flocculation point is the quantity of *n*-heptane required to generate maximum light linked with the start of asphaltene grouping (Mohammadi et al. 2017). One practical way to assess crude oil's overall stability is by using a precipitation agent (usually a straight-chain alkane like *n*-heptane) to cause flocculation at right time (Garca and Carbognani, 2001). Because *n*-heptane dilutes the solution and prevents asphaltene deposition, the samples' absorption decreases. The abrupt increase in absorption that occurs when *n*-heptane is added to samples is caused by the development of asphaltene solid phase in the mixture. Every asphaltene precipitation test's flocculation began at minimum position of the curve (Oh et al., 2002; Aske et al., 2002; Jamaluddin et al., 1995).

2.1.3 Thermodynamics behavior and solubility of asphaltene

Asphaltene precipitation occurs primarily because of thermodynamic changes including pressure, composition, and temperature changes (Tavakkoli et al., 2014). Furthermore, solubility of asphaltene is altered in certain ways by injection of liquids and gases. According to solubility theory, asphaltene dissolves in crude oil and precipitates when its solubility drops below a predetermined threshold (Sisco et al., 2018). Stability of asphaltene is impacted by variations in reservoir conditions. Asphaltene envelope can be used to determine asphaltene stability (Fakher et al., 2020). A thorough understanding of properties and behavior of asphaltene is also necessary for managing and preventing issues with its deposition at the oilfield.

According to thermodynamic behavior of asphaltene particles, asphaltene fraction is separated from crude oil when asphaltene precipitation starts. Asphaltene behavior with variation in medium's temperature and pressure can be explored using the asphaltene phase envelope presented in Figure 2-3. When the pressure is reduced to the bubble point, the amount of precipitated asphaltene reaches its peak. Below the saturation point, gas phase evolution and a decrease in density are expected.

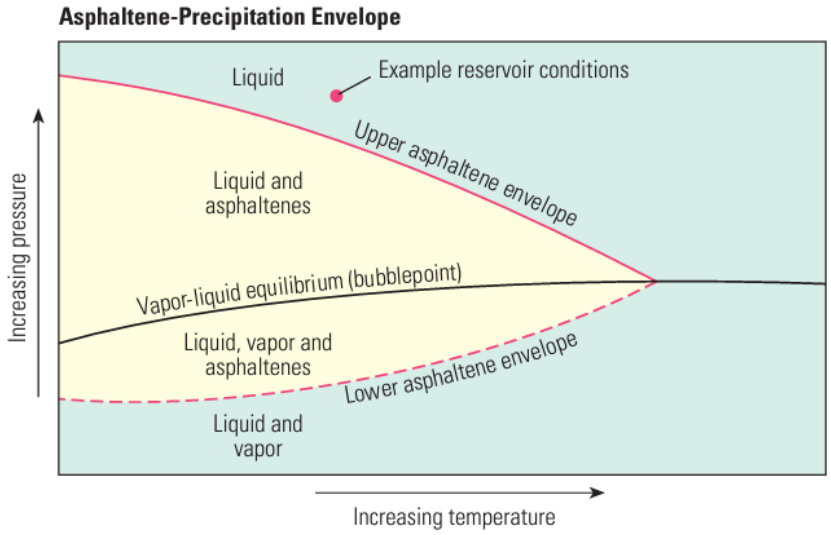

Figure 2-1: Schematic of asphaltene phase envelope (Akbarzadeh et al. 2007).

2.1.4 Asphaltenes properties: Composition, structure, and molecular weight

Ahmed et al. (2023) define asphaltenes as complex mixtures of heterogeneous molecules that are highly polydisperse in size and chemical composition includes metals like iron, nickel, and vanadium, as well as chains, polynuclear aromatics (polycondensed aromatic rings), aliphatic and naphthenic rings, and heteroatoms like oxygen, nitrogen, and sulfur. Asphaltenes typically have varying H/C and S/C ratios, but their N/C and O/C ratios are relatively constant. Atomic ratio analysis of asphaltenes from different crude oil samples is presented in Table 2-1 (Leyva et al., 2013).

Table 2-1. Atomic ratio analysis of asphaltenes from different crude oil samples (Leyva et al., 2013).

Asphaltene	**A-33**	**A-21**	**A-16**	**A-13**	**A-10**
	Atomic ratios				
H/C	1.250	1.106	1.226	1.220	1.215
S/C	0.033	0.038	0.037	0.043	0.065
N/C	0.011	0.013	0.011	0.012	0.011
O/C	0.001	0.001	0.001	0.001	0.002

Asphaltene molecule structure models are highly dependent on composition of elements such as alkyl and aromatic functional groups. Two main types of molecular models are proposed:

island and archipelago as shown in Figure 2-2 (Mullins, 2005). The average asphaltene compound in the island model is classified as a large polycyclic aromatic/heteroaromatic core ornamented with long alkyl chains and peripheral functionality with a molecular weight of 500 to 1000 g/mol and consist of 6 to 7 aromatic rings. A typical asphaltene constituent, according to the archipelago model is composed of two or more smaller, interconnected, polycyclic aromatic or heteroaromatic islands connected by saturated alkyl bridges and further covered with heteroatom functionality and short alkyl side chains of 5-7 aromatic rings with a molecular weight of roughly 6000 g/mol (Scott et al., 2021; Mohammed et al., 2021). According to Gray et al. (2021), asphaltene molecular weight in crude oils varies between 700-15,000 g/mol.

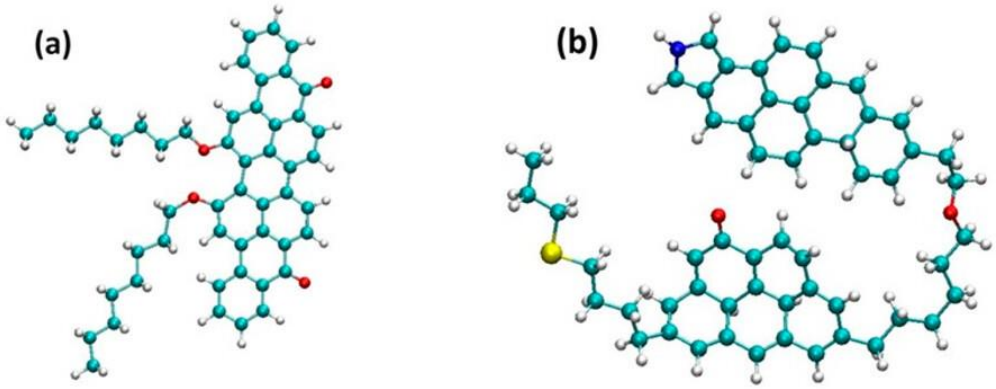

Figure 2-2. Models of asphaltene molecules: (a) island structure, (b) archipelago structure (Ali et al., 2023)

2.1.5 Asphaltene aggregation

The modified Yen model, illustrated in Figure 2-1, shows the nano-architectures of asphaltene molecules. Although asphaltene from various reservoirs worldwide typically exhibit similar compositions, variations in asphaltene concentration and the composition of residual oil give rise to distinct aggregate structures in different reservoirs (Mullins et al., 2015). The primary molecular framework of asphaltene comprises a singular, relatively substantial polycyclic aromatic hydrocarbon (PAH), accompanied by peripheral alkanes. Asphaltene molecules coalesce into nanoaggregates, generating aggregation numbers of approximately six along with a solitary disordered stack. These nanoaggregates further assemble into clusters with an estimated aggregation number of eight (Mullins, 2011).

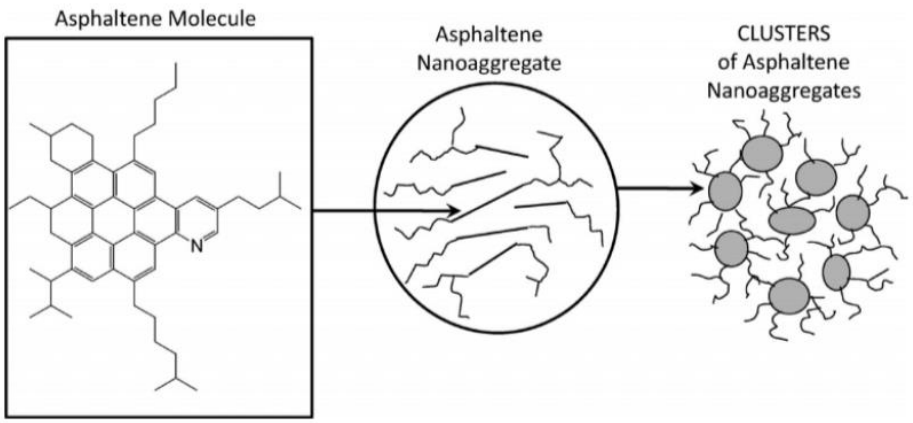

Figure 2-3. Modified Yen model (Mullins, 2010).

While the origin of asphaltene, the matrix in which they are found, and the prevailing physical conditions collectively influence asphaltene aggregation, these substances typically manifest as a dispersion of nanoaggregates at concentrations exceeding 50–100 mg/L (and occasionally as low as 20-50 mg/L) (Adams, 2014). Research indicates that the tendency of asphaltene molecules to aggregate in a pure solvent is markedly contingent upon their concentration (Speight, 2006). At lower concentrations, such as below 50 mg/L, asphaltenes are believed to exist either as oligomers of asphaltene molecules or as molecularly dispersed entities within solvents like toluene (Mullins, 2010). The self-assembly of asphaltenes predominantly occurs within toluene solutions. There is strong likelihood that similar complexation phenomena manifest in crude oil, attributable to toluene's superior solvent properties for asphaltenes compared to those of crude oils, coupled with the significantly lower aggregation thresholds observed in toluene relative to the typical asphaltene concentrations in crude oils (Mullins, 2008). The clustering of asphaltenes has been correlated with abrupt alterations in solution characteristics such as surface tension (Rogel et al., 2000) or heat of dissociation (Andersen and Christensen, 2000) arising from fluctuations in asphaltene concentration.

Although the constitution of crude oils is very complex but its constituents can be categorized into four primary fractions known as SARA: Saturate, Asphaltenes, Resins, and Aromatics. Resins and aromatics act as solvents; while, saturate compounds are deemed non-solvents with regard to their capacity to maintain asphaltene solubility. According to the micellar theory, asphaltenes and resins form stable associations within crude oils, existing in a state of equilibrium in terms of solubility (Maqbool et al., 2011; Matsushita et al., 2004). Resins are

considered as an important component to stabilize asphaltenes as they can bridge the solubility disparity between the polar asphaltenes and the nonpolar saturates in the oil matrix via production of micelle-like structures (Mullins et al., 2007). Asphaltene precipitation commonly arises due to medium instability induced by a disruption in the colloidal structure, facilitating phase separation phenomena. Notably, among the fractions within crude oil, only the asphaltene fraction exhibits a correlation with API gravity: heavier crude oils (lower API) tend to harbor higher asphaltene contents. Conversely, lighter crude oils typically contain saturate substances in higher concentrations. However, no conspicuous trend emerges concerning API gravity concerning resin and aromatic content (Guzmán et al., 2020).

The Colloidal Instability Index (CII) regards the crude oil system as a colloidal solution made up of SARA pseudo-components. It may be theoretically described as the ratio of the total contents of saturates and asphaltenes to total contents of resins and aromatics. Eq. 2-1 can be used to compute CII (Ashoori et al., 2017):

$$CII = \frac{(\text{Saturates in wt\%}) + (\text{Asphaltenes in wt\%})}{(\text{Resins in wt\%}) + (\text{Aromatics in wt\%})} \qquad \text{Eq. 2-1}$$

The stability assessment criteria to ascertain the stability of crude oils are as follows: Crude oil is classified as unstable if its CII value is < 0.9 and stable if its CII value is greater than 0.9. Crude oil falls into the unclear zone if the CII value is between 0.7 and 0.9 (Asomaning and Watkinson, 2000).

2.1.6 Impact of operational parameters and reservoir condition

Temperature (T), pressure (P), and fluid composition (X) are examples of process and operational parameters that affect asphaltene precipitation. The assessment of stability is influenced by chemical composition of crude oil. Low hydrogen concentrations and increased aromaticity are characteristics of unstable crude oil asphaltenes (Rogel et al., 2001). Asphaltenes might become more soluble at higher temperatures and lower pressures, leading to less precipitation (Tavakkoli et al., 2014). Heating causes a change in the composition of crude oil. Light fractions, primarily the alkanes, dilate, and lower the solubility parameter of crude oil, which makes asphaltenes less soluble (Gharbi et al., 2017).

2.1.7 Asphaltene precipitation mitigation measures

Asphaltene precipitation during oil production leads to a number of issues. Several measures are put into place to address the deposition issue, which significantly reduces the oil production rate. Treatment methods include using bacteria, heat, chemicals, mechanical, and ultrasonic (Gharbi et al., 2017). Among the chemical additives, asphaltene deposition inhibitors and dispersants are widely investigated in the literature (Oschmann, 2002; Gupta et al., 2009). Asphaltene inhibitors prevent asphaltene molecules from aggregating because they have the ability to alter the flocculation pressure of asphaltenes. It is possible to move the asphaltene precipitation in the well to a location in the production system where it will be easier to treat (Marques et al., 2004; Smith et al., 2008). Nonpolymeric surfactants make up the majority of commercial dispersants, in use to minimize size of the flocculated asphaltene particles (Kelland, 2016). These dispersants spread the flocculated asphaltene particles to keep them suspended in crude oil, but they have no effect on AOP (Asomaning and Yen, 2002).

2.2 Adsorption isotherm models

2.2.1 IUPAC classification

To understand how asphaltenes stick onto NPs, scientists have proposed different ways of to explain the processes involved. Models are developed that predict how well an adsorption process works though matching the models with experimental data. International Union of Pure and Applied Chemistry (IUPAC) has suggested a classification scheme for adsorption isotherms as shwon in Figure 2-2 (Thommes et al., 2015). Modeling the equilibrium adsorption of asphaltene onto NPs using various adsorption isotherms, Type 1, Type 2, Type 3, Type 4, Type 5, and Type 6, and discussing these isotherms along with their parameters and properties, including hysteresis enables understanding the adsorption process.

The IUPAC adsorption type curves can also be applied to model adsorption kinetics of asphaltene onto NPs/NCs. The classification of isotherm types provides insight into pore structure of materials under investigation. Type I(b) isotherms correspond to materials featuring a broad pore size distribution, encompassing wider micropores and potentially small mesopores (≤2.5 nm). Conversely, type I(a) isotherms are characteristic of microporous materials primarily composed of narrow micropores (with widths <∼1 nm). Type 2 isotherms stem from adsorption onto

macroporous or nonporous adsorbents. Notably, type 3 isotherms lack a discernible monolayer, indicating weak interactions with the adsorbent. Type 4 isotherms depict adsorption onto mesoporous materials, with type 4(a) isotherms specifically indicating capillary condensation with hysteresis, typically observed when pore widths exceed a critical threshold. The completely reversible type 4(b) isotherm elucidates the adsorption behavior on adsorbents featuring narrower mesopores. Isotherm type 5 bears resemblance to type 3, indicative of feeble interactions between the adsorbent and adsorbate within a limited range of relative pressures. Isotherm type 6 captures the phenomenon of stepwise multilayer adsorption occurring on a homogeneous non-porous surface.

2.2.2 Langmuir isotherm model

Adsorption by Langmuir adsorption isotherm model can only take place at a fixed set of specific localized sites that are identical and do not have any lateral interactions with the molecules being adsorbed. This monolayer adsorption assumption leads to the assumption that the layer of adsorbed molecules is one molecule thick. The term "Langmuir isotherm" refers to homogenous adsorption, in which all adsorbate-binding sites have an equal affinity and all molecules have similar enthalpies and adsorption activating energies. Graphically, this is represented by a plateau or equilibrium saturation point, where additional adsorption is not possible once a molecule occupies a site as shown in Figure 2-2I(b). Furthermore, the quick reduction in molecules attractive interactions has been linked by Langmuir model to an increase in distance. This is how the Langmuir isotherm model is represented (Langmuir, 1916):

$$q_e = \frac{Q_m b C_e}{1+bC_e} \qquad \text{Eq. 2-2}$$

where b is a constant for Langmuir isotherm and Q_m is the adsorption capacity. The quantity of asphaltene adsorbed per unit weight of adsorbent is denoted by q_e, and the rest of the asphaltene concentration in the solution is indicated by the value C_e.

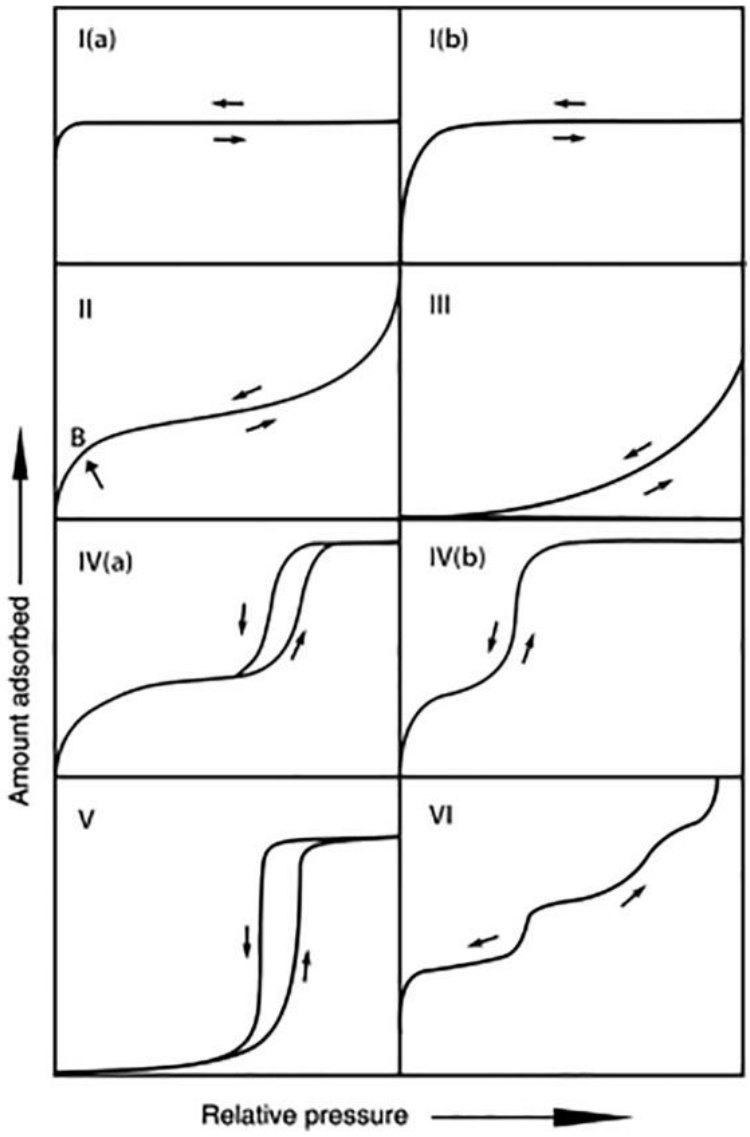

Figure 2-4. IUPAC classification curves for adsorption isotherm models (Mazloom et al., 2020)

2.2.3 Freundlich isotherm model

The oldest known formula for non-ideal and reversible adsorption, including layer formation, is the Freundlich isotherm model. Applying this experimental model to multiple adsorption layers with irregular heat generation and affinity distribution across a diverse surface is possible. On polarized porous surfaces, the Freundlich isotherm is frequently used in heterogeneous cases, particularly for organic substances or highly interacting species. The Freundlich isotherm model is expressed by using the following equation (Freundlich, 1906):

$$q_e = k_F C_e^{\frac{1}{n}}$$ Eq. 2-3

where *n* and *k* are the Freundlich constants, q_e is adsorbent quantity, C_e is the material's concentration is not adsorbent.

2.3 Nanotechnology

Nanotechnology is science of material functions and capability at atomic or nanoscale (10^{-9} meters) (National Nanotechnology Initiative, 2015). It provides possibility to develop advanced materials with increased surface area, and improved interaction forces, physical, mechanical, and chemical properties which is not feasible in macro scale (Khan and Hossain, 2022). Nanotechnology is a significant driving force of technological changes in biological sciences, cognitive research, and technology for information. These changes are expected to affect the petroleum industry in future, as well. Although, the research on application of nanomaterials in oil and gas engineering has been going on for more than two decades and some filed trials have also been reported.

2.3.1 Nanoparticles application in oil and gas industry

Nanotechnology offers innovative solutions to boost productivity, reduce costs, and solve some environmental issues in petroleum industry including drilling, EOR, production and exploration (Kong and Ohadi, 2010). The theoretical and experimental investigations of nanotechnology applications in petroleum industry is increasing year after year. Especially, potential uses of engineered nanomaterials in the oilfield (Agista et al., 2018). Nanotechnology research and application is in high demand in the upstream and downstream processes due to the accuracy and efficiency (Mansoori et al. 2005).

2.3.2 NPs/NCs for inhibition of asphaltene precipitation

Using flocculation inhibitors represents a viable approach for mitigating asphaltene precipitation. These inhibitors facilitate smoother asphaltene production by modulating flocculation pressure to alternative levels (Marques et al., 2004; Smith et al., 2008). Hence, it is more practical to prevent asphaltenes from depositing by using NPs thanks to their adjustable features and properties such as a functionalizable surface, high degree of dispersion, high mobility in porous media, potential catalytic activity, high surface area, and high adsorption capacity (Franco et al., 2013).

SiO_2 NPs and Xanthan natural gum as a polymer have been used in some EOR and asphaltene precipitation research works reported in the literature. Ahmadi and Aminshahidy (2018), reported that SiO_2 NPs reduced asphaltene content during experiments from 0.56 wt% and 1.10 wt% to 0.27 wt% and 0.52 wt%, respectively. SiO_2 NPs with about 20 nm size stopped asphaltene particles from sticking together (Li et al., 2018). By sticking to the clusters in the solution, silica NPs make them smaller, but not all of them stick the same way (Nassar et al., 2015). Betancur et al. (2016) reported that when size of SiO_2 NPs gets bigger, then their adsorption capacity reduces because the NPs are unable to adsorb more asphaltene. SiO_2 is a popular NP for making mixtures with other NPs, polymers, and surfactants because of its exceptional features. According to Hosseini-Dastgerdi et al. (2024), SiO_2-Polyacrylamide (PAM) NC has more vacant sites available for asphaltene adsorptions leading to a higher adsorption capacity.

2.3.3 Mechanism of asphaltene nano-inhibitors

The interactions between asphaltene and NPs are governed by the same aggregation mechanisms that regulate asphaltene self-association. However, the attractive forces exerted by asphaltenes on NPs' surface surpass those the between asphaltene molecules themselves (Montes et al., 2019). This phenomenon can be attributed to two primary factors: firstly, the active sites present on the NP's surface typically consist of chemical species characterized by high dipole moments (Soler et al., 2023). Secondly, the asphaltene structure inherently possesses fewer surface-active groups compared with surfaces of nanoparticulated sorbents (Adams, 2014). The adsorbed asphaltenes develop a monolayer configuration upon interaction and subsequent adsorption onto the NP's surface until their active sites become inaccessible due to either saturation or steric hindrance effects (Betancur et al., 2016). The interaction between unbound asphaltenes and those within the monolayer is primarily driven by π–π stacking (Adams, 2014). Furthermore, because of steric effects, the adsorbed asphaltenes may engage in interactions with free asphaltenes present in the crude oil. The multilayered assembly of asphaltene adsorption occurs due to asphaltene aggregation on the surface of the NP (Guzmán et al., 2016). A simplified representation of asphaltene-NP attraction is shown on the left side. Individual asphaltene molecules are adsorbed onto surface of the NP forming a monolayer. Additional layers of asphaltene molecules accumulate on the surface of the NP forming a multilayer adsorption system (right side).

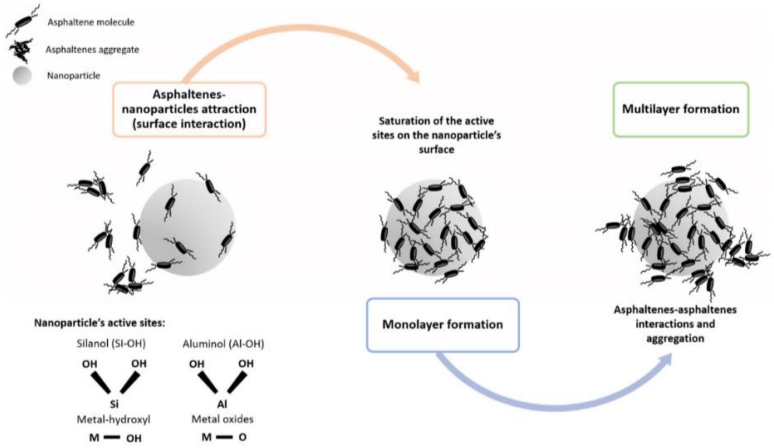

Figure 2-5. Mechanism of asphaltene adsorption onto the surface of NPs (Guerrero-Martin et al., 2023).

2.3.4 Applications of SiO_2-KCl-Xanthan NC

Application of SiO_2-KCl-Xanthan NC for EOR and making smart drilling fluids has been reported in the literature with excellent results (Ali et al., 2022; Motraghi et al., 2023). Motraghi et al. (2023) reported application of ethanol and methyl ethyl ketone solvents alone or together in a new mix is an effective way for IFT reduction and wettability alteration as EOR mechanisms. This created a synergy between the solvents and SiO_2-KCl-Xanthan NC. Some other researches are reported on formulation of smart drilling muds using SiO_2 NPs and various polymers such as HV-CMC, xanthan gum, LV-CMC, and salts (KCl, NaCl) at 25°C. Depending on how much SiO_2 NP is added and what type of salt and polymer is used, created smart muds with different enhanced properties. (Belayneh and Aadnøy, 2016). All these tests show that NCs play have a high position in oil and gas related research. The rheological and filtration properties of drilling fluids was enhanced by adding KCl (Ali et al., 2022).

2.3.5 Asphaltenes adsorption onto metal oxide NPs

When asphaltenes is adsorbed onto surfaces, the adsorption process also depends on chemistry of the surface in addition to the chemical composition of the asphaltene and its origin and structure (Adams, 2014). Adsorption capacity for certain asphaltenes exhibits considerable variation across various sorbents. On the contrary, adsorption of some other asphaltene sources remains relatively unaffected regardless of the type of sorbent used (Xing et al., 2010). Some it has been reported in the literature that affinity, adsorption capacity, and selectivity across diverse sorbents exhibit less

sensitivity towards the source of asphaltenes (Dudášová et al., 2008). Acoording to Rudrake et al. (2009), asphaltenes exhibit capability to adsorb onto surfaces either as individual particles or as colloidal aggregates with varying sizes. This accumulation of material culminates in the formation of solid deposits, which have the potential to obstruct industrial equipment and pipelines. Moreover, asphaltenes possess the tendency to adsorb onto the surface of reservoir rocks, consequently yielding deposits that can modify the wettability of the mineral surface and impede the extraction of crude oil from the reservoirs (Saraji et al., 2010).

Adsorption of asphaltene by NiO NPs depends on the type asphaltene precipitant. Eexistence of heteroatoms in asphaltene causes them to be polar, leading to greater contacts (Nassar et al. 2011). Addition of NiO NPs significantly reduced the oxidation T and activation energy, demonstrating their catalytic effect (Ezeonyeka et al. 2018). Asphaltene adheres better onto NPs when there is a high *n*-heptane content resulting in less asphaltene flocculation and precipitation (Kazemzadeh et al. 2015). Unclear and contradicting! Very small size of NPs enables external adsorption without intra-particle diffusion, the adsorption rate is high (Nassar et al. 2010). The initial asphaltene concentration, T, H/T ratio, and water content influenced rapid pseudo-second-order model-based asphaltene adsorption onto the NPs. Pure asphaltene exhibited a greater capacity for adsorption than bitumen or maltenes, indicating that the chemical make-up of the oil ingredient as well as its molecular size and structure play a role in adsorption (Nassar et al. 2010).

Adsorption of asphaltene using NiO NPs causes a reduction in their exposed surface area and diminishes the asphaltene uptake. Because of poor dispersion of NiO NPs, asphaltene adsorption by NCs is somewhat higher (Cortés et al. 2012). Variations in particle size and chemical compositions of the NPs affect the adsorption properties. Alumina, rocks, and silica gel failed to demonstrate a substantial affinity for asphaltene adsorption by surface uptake. Such outcomes might be a result of the chemistry and functionality of the molecular structure and surface properties (Franco et al. 2013). Strong hydrophilic properties of NiO_2 NPs justify its good performance in asphaltene adsorption (Dudaśovă et al. 2008). Increasing the NiO concentration in NCs causes an increase in adsorption of asphaltene at isothermal condition (Cortés et al., 2012). During the adsorption process, the acidic surface increases the affinity for asphaltene but also increases the estimated activation energy (EAE) and reduces catalytic effects (Franco-Ariza et al. 2016). According to Nassar et al. (2011), the level of contact between asphaltene and NP's homogenous surface causes variations in adsorption affinity. Increasing the acidity of the NP's

surface results in improved affinity for asphaltene. Asphaltene adsorption onto NP is an exothermic process. Temperature has a significant impact on how big is the asphaltene aggregate. Asphaltene absorption reduces as T increases and size of the aggregate shrinks (Nassar, N. 2010).

Cortés et al. 2016) reported that silica NPs absorbed more asphaltene compared with micro size particles because of their large surface area and dispersibility. Presence of NPs with enough porosity increases the size of adsorption region and prolongs the time it takes to stabilize, which is advantageous for asphaltene adsorption (Wang et al., 2022). Asphaltenes appear to adhere to the given NPs by electrostatic force and pH interaction, which appear to be the main driving forces (Hosseinpour et al., 2013). The quick completion of asphaltene adsorption onto Alumina-SHS makes it suitable for in situ upgrading and shows a significant increase in asphaltene absorption with greater NiO loading (Franco et al., 2013). SNi1Pd1 NPs compared with fumed silica alone, their asphaltene adsorption increased and degree of asphaltene self-association was reduced. This suggests that these NPs have the capacity to hinder self-association of asphaltene (Cortes et al., 2012).

2.3.6 Factors affecting adsorption of asphaltene onto NPs/NCs

NPs have a greater surface area per mass as their size gets smaller. Asphaltene molecules can adhere to the surface of NPs when there is more contact area is available. In the case of smaller NPs, this most likely causes asphaltene to adhere quicker. Thus, for the same amount of NP, small NPs may be able to absorb more asphaltene. The main reason is that smaller NP have less weight and more energy that makes them better adsorbents (Mazloom et al., 2020). Variations in mixing process of NP with asphaltene also effects the adsorption process. NP interaction force with asphaltene is higher when they have a similar structure (Madhi et al., 2017). Adsorption effectiveness also depends on asphaltene concentration (Ansari et al., 2022).

2.3.7 Limitations of nano-inhibitors for asphaltene

Different NPs have different adsorption capabilities. However, depending on specific circumstances and asphaltene concentration, the overall adsorption capacity of NPs may be still limited (Nassar et al., 2011). At high temperatures, the effectiveness of NPs may be also limited (Shojaati et al., 2017). However, there is usually no extreme temperature encountered in conventional crude oil reservoirs. Various fluid flow parameters could be impacted by the decrease in surface tension among oil and gas in the event of NPs (Hassanpour et al., 2018). Although the

inclusion of NPs enhances stability and partially prevents precipitation, full avoidance of asphaltene deposition could not be possible only by the addition of NPs (Parsaei et al., 2020).

2.4 Nano-inhibition efficiency evaluation tools

There various experimental approaches for measuring the asphaltene onset point have been investigated. AOP corresponds to the concentration of precipitant at which deposition of asphaltene starts. As a precipitant meant different volumes of *n*-heptane. In other words, the onset point is referred to the minimum volume of the precipitant needed to measure an established quantity of synthetic oil while unstabilized asphaltene particles starts precipitate out of the solution. The useful aspects, working procedures and potential outcome of laboratory approaches including UV-vis spectroscopy and thermogravimetric analysis (TGA) to determine AOP is discussed in the following section.

2.4.1 UV-vis spectroscopy for AOP determination

The indirect methods for determining the amount of asphaltene imply that it has been deposited/adsorbed on solid surfaces. The indirect approach works by removing unstable asphaltenes through centrifugation, which alters the optical density of the residual liquid. UV-vis spectrophotometry can be used to determine the concentration of an asphaltene solution following exposure to metal particles. Asphaltene adsorption on metals is determined by the difference between the starting and final concentrations (Alboudwarej et al., 2002). UV-vis spectrophotometry can be used to quantify the extent of asphaltene deposits in the stainless-steel tube (Arsalan et al., 2014).

The working principle of spectroscopy based on the ultraviolet pathway of a different range of spectrum through adsorption detection of the monochromatic light by colorless substances. This method can be applied either for solution or as a solid substance. The difference of light energy passed through the baseline state and the material’s state offers the absorbance value. The absorbance of transmitted light is plotted as a function of n-heptane concentration. During the early phases of the titration experiment, there was an initial drop in light absorbance, which was caused by the precipitant's diluting impact before its concentration reached the threshold value required for asphaltene precipitation. When the precipitant concentration reached a certain threshold, the asphaltene particles precipitated out of the solution and absorbed the light flowing through. This

local minimum point was known as the onset of asphaltene precipitation. According to the Figure 2-6 the AOP can be observed at 40 vol% of *n*-heptane.

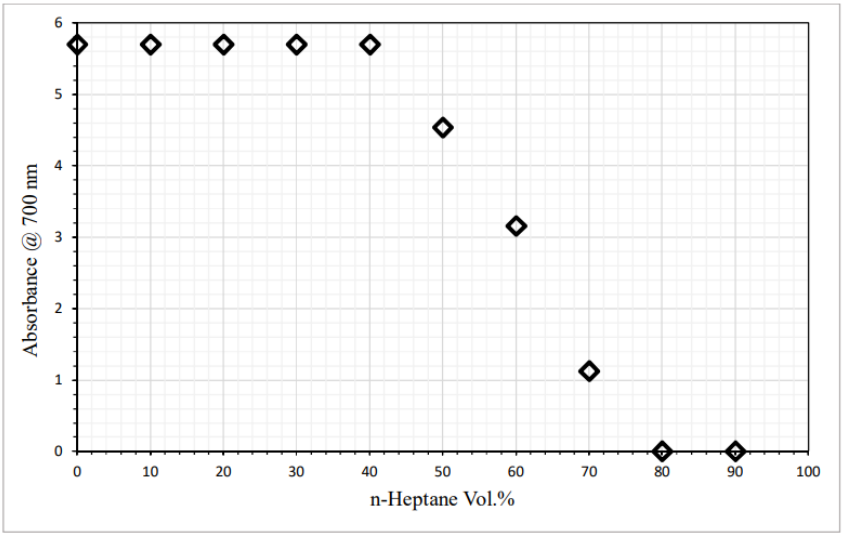

Figure 2-6. Determination of onset point for the synthetic oil with 0.5 wt. % of asphaltene in the absence of nanoparticles after modification of the dilution effect obtained with indirect technique (Shojaati et al., 2017)

As shown in the Figure 2-7 by adding of different nanoparticles with same concentration the AOP is shifted to the right hand side. It means that the n-heptane value of threshold point is increased. By adding Al_2O_3 it is shifted to the 58 vol%, Fe_3O_4 is raised the n-heptane value to the 48 vol% and at NiO NP the AOP started only at 53 vol% of *n*-heptane concentration. In this case the most optimum and effective adsorption nanoparticle with 0.1 wt.% concentration was Al_2O_3. The adsorption potential can be measured and compared with different NPs or different concentration of one singular NC.

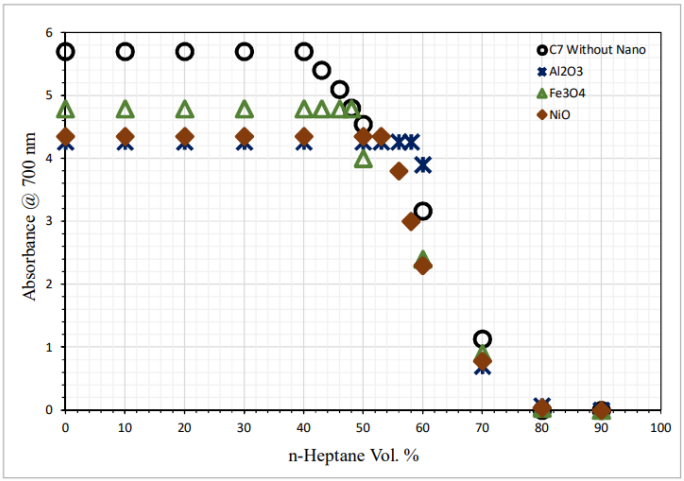

Figure 2-7. Determination of onset point for the synthetic oil with 0.5 wt. % of asphaltene in the presence of metal oxide nanoparticles with 0.1 wt. % (Shojaati et al., 2017)

2.4.2 Thermogravimetric analysis

Thermogravimetry analysis determines changes in weight of a material over time or at different temperatures. The sample can lose weight when is heated or cooled under monitored change profile. The mass change outline and heat flow of a sample can be evaluated under predetermined conditions up to specific temperature. As a result, TGA is mostly used to explain certain thermal events, such as adsorption (Loganathan et al., 2017).

The TGA curve is often a representation of weight change over time or at a specific temperature. Figure 2-8 illustrates an average TGA curve. The TGA curve in Figure 2-8 shows multiple stages of decomposition. This decomposition could be caused by drying, which evaporates volatile substances and causes desorption. The initial decomposition temperature can be identified when weight change becomes visible with a significant decline. The final decomposition temperature may be recognized when weight change reaches its highest level and cannot fluctuate any further. In figure 2-8 the initial temperature of sample after adsorption is 229.92 ˚C and final temperature is equal to 400 ˚C.

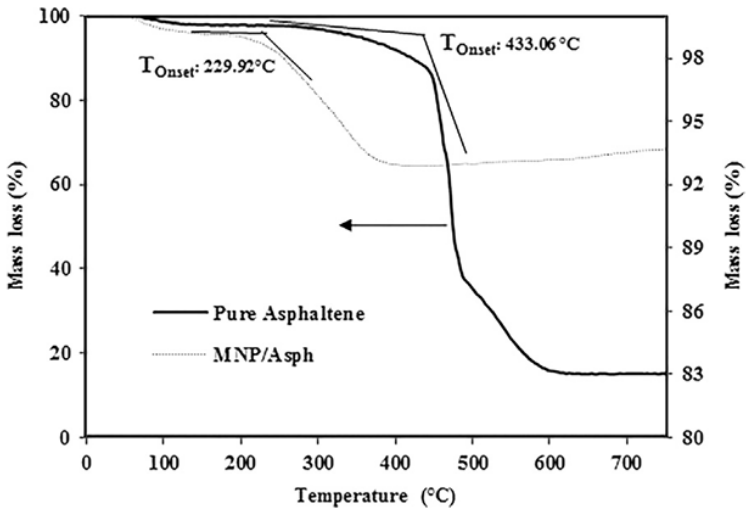

Figure 2-8.

Figure 2-8. Mass loss as a function of temperature for asphaltene with and without maghemite nanoparticles (Mirzayi and Shayan, 2014)

In addition to predicting sample thermal stability, TGA can be used to analyze the kinetics of adsorption at diverse conditions. To explore kinetics, it is necessary to optimize the components or settings that affect samples mass change across the testing time. The weight of the sample used for investigation and the rate of heating have been determined to affect mass change.

2.5 Nanocomposite characterization tools

Due to the complexity of the physical and chemical processes involved, there is no one revealing characterization method for nanomaterials. A variety of property measures must be developed and used in order to complete the characterization. The following paragraphs will explain how to examine them using microscopy, surface analysis, dispersion, morphology analysis and molecular identification.

X-ray diffraction (XRD)

X-ray diffraction is applied to determine the chemical content of nanomaterials as well as their crystalline structures. In the instance of NC characterization, X-ray diffraction measurements provide an indicator of the extrapolate information on the position of the organic molecules in the scattering region (Mittal et al., 2011).

Fourier Transform Infrared Spectroscopy (FTIR)

The working principle of FTIR technique is based on the measuring of absorption process of infrared light caused by vibrational movements in molecules of the nanomaterial. The different distinctive peaks of the vibration in spectra help identify substances. The primary applications of FTIR are structural determination, functional group investigation, qualitative-quantitative characterization (Castellon et al., 2013).

3 MATERIALS AND METHODS

Quality of research data highly depends on the methodology used for sample preparation and testing. The characteristics of the materials used in this research work including the heavy crude oil, NC, and solvents are described. Then, asphaltene extraction method (IP-143 standrad) and asphaltene and NC characterization techniques including XRD, FTIR, DLS, SEM, TGA, and BET are described, briefly. To assess the efficacy of the nano-inhibtor for asphaltene adsorption and inhibition, systematic procedures for sample preparation and testing using UV-vis spectrophotometer and TGA analysis methods are described in details.

3.1 Materials

3.1.1 Heavy crude oil sample

A paraffinic heavy crude oil from West Kazakhstan was used to extract asphaltene. Density of the heavy crude oil is 0.946 g/cm^3 and dynamic viscosity of the heavy crude oil at 25°C was determined 153 cP. The asphaltene content was around 24.4-25.6%.

3.1.2 SiO_2-KCl-Xanthan NC

Dr. Shafiei provided the SiO_2-KCl-Xanthan NC used in this research work. The procedure for synthesis of the NC can be found in the literature that is briefly described in this section. The SiO_2-KCl-Xanthan NC was synthesized and used as the nan-inhibitor in this research work. The NC was synthesized using the procedure described in the previously published papers from the literature. The NC's components are KCl, SiO_2 and Xanthan gum that have been used before for EOR and drilling fluid research. Na_2SiO_3, xanthan gum, KCl, ethanol, and plant extract from Euphorbia condylocarpa were used to synthesize the NC. To correct the pH, NaOH was also added to the mixture (Khaksar Manshad et al., 2023). Synthesis started with extraction at 80°C for 30

min of the solution from the mixing process of 100 g of dried leaves of the Euphorbia condylocarpa plant with 500 mL of distilled water. NP making procedure then continued with mixing for 10 h at 10 pH environment and 80°C temperature of 5 g of Na_2SiO_3 and 100 mL of the collected extract. The solution was then stirred until a dry precipitate was obtained and then mixed with KCl-hydroalcoholic with volume of 100 mL under the same experimental condition. The precipitated powder product of SiO_2 and KCl mixed with 10 g of Xanthan gum. Refluxing was used for 5 h in ethanol. The refluxed nanopowder was then dried (Ahmadi et al., 2022).

3.1.3 Solvents

n-heptane was used for asphaltene extraction precipitation tests. Pure C_7H_{16} provided by Ekos-1 (TS 2631-023-444931179-98) was used in asphaltene extraction process and preparation of synthetic crude oil. The toluene was provided by Sigma-Aldrich and ACS reagent with >99.7 (GC), formula: C_7H_8, MW: 92.14 g/mol, and density: 0.865 g/mol at 25°C.

3.2 Methods

3.2.1 Asphaltene extraction

The IP-143 standard was used to extract the asphaltene: First, the crude oil was dissolved in *n*-heptane with a ratio of 1:40 (Alboudwarej et al., 2002). After about 4 hours of dissolving, *n*-heptane separates asphaltene from the crude oil. Then, the solution containing asphaltene goes through filtration process. Whatman #42 filter paper was used to separate the asphaltene from solution. This step helps to purify the asphaltene further by isolating it from rest of the solution. Soxhlet extraction device was then used in the subsequent extraction step. In Phase 1, heated *n*-heptane is refluxed with the filtered solution that contains contaminants like wax and leftover asphaltene. The *n*-heptane collected at the bottom of the Soxhlet extractor was refluxed repeatedly until it turned clear and colorless. This stage aids in removing contaminants from the mixture. The residual pollutants, including the asphaltene stocked to the filter cake, are dissolved using hot toluene in Phase 2 of the Soxhlet extraction process. The asphaltene is successfully removed from the filter paper by dissolving the contaminants, allowing for additional purification. Toluene is then eliminated by carefully heating the solution, which allows for the isolation of the pure asphaltene. The asphaltene and toluene solution is evaporated in an oven heated up to 80°C as the last stage. One day is spent on this evaporation process, allowing the toluene to progressively

disappear and be replaced by pure asphaltene. Scheme of the asphaltene extraction process is illustrated in Figure 3-1.

3.2.2 Synthetic oil preparation

The asphaltene was collected from the bottom of the beaker and transferred to a separate jar. Weighing a specific weight of asphaltene, it was mixed with acceptable volume of toluene in a larger jar. The mixture was stirred using a magnet on a magnetic stirrer for 4 hours at 300 rpm to prepare synthetic crude oil.

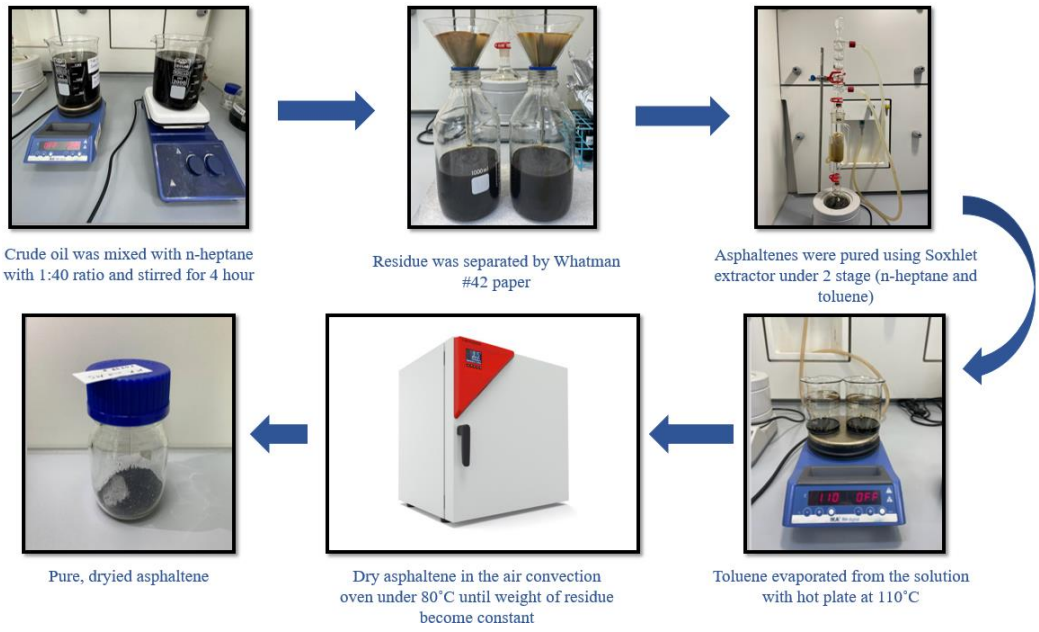

Figure 3-1. Scheme of asphaltene extraction procedure according to IP-143 standard.

3.2.3 Characterization of asphaltene and NC

In this section, asphaltene and NC characterization methods are described, briefly. Understanding the characteristics of the asphaltene and the NC is crucial for understanding of particle interaction mechanism and adsorption features. Key features of the NC such as surface area, crystallite and particle size and its distributions, bound force types of the chemical compound, pore volume, surface morphology, and chemical composition are measured. Each section includes a brief summary of the experiment steps, working principle of the tools used, and the raw data analysis procedure.

3.2.3.1 Fourier-transform infrared spectroscopy (FTIR)

The FTIR analysis was performed using a Nicolet iS10 FT-IR spectrometer. The infrared spectrum measurement range varies between 400 and 4,000 cm^{-1} wavelength. The spectrometer works based on the Fourier Transform Infrared Analysis. Chemical functional groups and bonding type of the NC are identified.

A background spectrum is first collected from the local air infrared spectrum. Following measurements responses based on this baseline, any deviations from the spectrum straight-line especially high peaks means certain functional groups. They are evaluated by their peak value and wavelength. The instrument generates SPA and CSV files from recorded background spectrum, which are saved for later examination. Next, the sample is placed in path of infrared beam, ensuring it is positioned correctly for accurate analysis. Pressing the "sample" button on FT-IR spectrometer saves spectrum of the sample, measuring transmission or absorption of the infrared radiation to reveal the details about its molecular vibrations and functional groups. After measurement of each sample, the work area is cleaned again with ethanol or another suitable cleaning solution to remove any remaining contaminants or residues. Repetition of the aforementioned procedures will ensure that FTIR of each sample is measured correctly.

3.2.3.2 X-ray diffraction (XRD)

XRD is used to determine crystallite size, lattice parameters, phase, and structure of materials. The composition of particles can be discovered using reference patterns given in the database of International Centre for Diffraction Data, since they correlate with the strength and location of the peaks from results.

Crystallite size of the NC might be determined using the Debye-Scherrer equation (Mustapha et al., 2019):

$$D = \frac{k\lambda}{\beta \cos\theta} \qquad \text{Eq. 3-1}$$

where D is the crystallite size in nm, k is the Scherrer constant value which equal to the 0.9, X-ray diffraction tool wavelength is defined as λ and is equal to 0.15406 nm, β is the full width at a half maximum (FWHM) of the peak in radian, θ is the peak position in radian.

Based on the interaction of X-rays with the crystal lattice of the material, the device will generate X-ray diffraction patterns. The resulting peaks provide details about the sample's crystal structure and phase composition. Once the analysis is complete, ethanol is used to clean any glass lenses or spatulas used in the sample preparation process. Proper cleaning facilitates instrument hygiene and prevents potential contamination for subsequent sample procedures. All XRD findings from the analysis should be saved onto a flash drive or other suitable storage devices. These results will include diffraction patterns and related information that can be further examined and used.

3.2.3.3 Dynamic Light Scattering (DLS)

DLS is a useful technique for measuring NCs dispersed in solvents since it can give information about presence of aggregation and agglomeration as well as particle size (Linkov et al., 2013). It is an inexpensive, non-destructive, and non-intrusive process, and works quite quickly. Main challenge for samples that are polydisperse is interpreting the results (Kim et al., 2014).

Sampling and sample preparation: Samples are prepared using 30 cc of dispersion water and 0.015 g of NC. The solution is then diluted. The dilution process helps to ensure that NCs are evenly spread throughout the solution, allowing for accurate DLS measurement. It is possible that some of NC solutions have precipitated particles. Homogenizer is used to mix these solutions. Alcohol should be used to clean the homogenizer before use to avoid any potential contaminations. The homogenizer should then be inserted into the mixture. But it should be kept from being dropped to the bottom. The homogenizer was used for 15 minutes at 0°C. This cold treatment enables a uniform dispersion of the NPs in the solution and aids in breaking up any agglomerates. The solutions should be homogenized for 20 minutes in an ultrasonic bath. The ultrasonic bath uses high-frequency sound waves to disseminate the NCs evenly throughout the solution to break up any agglomerates. The scattered water without any NCs is measured to establish the background (baseline) for the solutions. This creates a baseline for subsequent tests and aids in separating the background noise from the NC signal. The main goal of such initial check is to confirm that the instrument is operating correctly. It also provides a measure of system repeatability using a "routine" sample.

NC solutions are diluted once more with dispersion water at suitable ratios, such as 1:100, 1:1,000, and 1:10,000, after obtaining the background. These dilutions enable the analysis of a

larger variety of particle sizes and shed light on the particle size distribution. Using the DLS device, measurements are done using the diluted solutions. For real-time visualization of Brownian Motion and electrophoretic mobility, the measuring size is 0 nm to 1,000 nm. For Zeta potential, the working range is −100 mV to + 100 mV; Conductivity is 8.75 μS/cm sensed.

The sample is injected gradually to prevent air bubbles in the cell, and analysis is not done until there is no air bubble inclusions left. Following the particle size observations, the related zeta-potential measurements are made right away. The device measures the time-dependent variation of scattered light resulting from the suspension of random Brownian motion caused by NCs via dynamic light scattering. The size information provided is derived from the particles' mean diameter, which is obtained by deducing and analyzing their diffusion coefficient. To determine the zeta-potential, the device measures the net velocity of the liquid's NCs because of applying an electric field using laser Doppler electrophoresis.

3.2.3.4 Brunauer-Emmett-Teller (BET) measurement

The surface area of NPs/NCs is calculated using the Brunauer-Emmett-Teller (BET) method. The chemical and physical adsorption of nitrogen gas onto the surface of the solid material underpins the BET technique by Nitrogen porosimeter. When characterizing the NPs/NCs, measuring the surface area is a crucial step. Because by surface area of NP it is easier to describe the level of adsorption. BET measurement is best method to find specific surface area directly without any formula calculation.

Sample preparation: Place the appropriate quantity of nanoparticles (NP) or nanocomposites (NC) in a crucible. Make sure the crucible can resist extreme heat. Place the crucible containing the sample inside the furnace and heat it to 400°C. Give the sample an hour to heat up to the desired temperature. This procedure aids in removing any residue or adsorbed compounds from the sample's surface. To completely rid the heated sample of any impurities or pollutants, thoroughly wash it with ethanol. For effective washing, one of two methods - a magnetic stirrer or an ultrasonic bath - is advised. However, using a magnetic stirrer should be avoided if the sample contains iron (Fe) to prevent interaction with the magnetic field. Use a centrifuge to separate the ethanol solution from the NP/NC sample after the ethanol-washing step. Centrifugation aids in separating the sample's liquid and solid phases, enabling additional processing. Place the sample that was obtained after centrifugation in a 60°C oven. Put the sample

in the oven to completely vaporize the ethanol. This process guarantees that any remaining solvent from the sample has been eliminated. Three to five times, repeat the ethanol washing, centrifugation, and ethanol evaporation methods mentioned above. The sample is thoroughly cleaned and any impurities or pollutants are removed thanks to this repetition. To achieve smaller particle sizes and to homogenize the nanocomposite, crush the sample once it has dried fully. This procedure improves the sample's surface area's accessibility for BET analysis.

Requirements for sample preparation for BET analysis:

- Sample weight: 0.2 to 1 gram
- Dry the sample
- The maximum temperature that will not harm the sample's structure is often selected to reduce the degassing duration. According to TGA data, the temperature should be up to 300°C.

3.2.3.5 Scanning electron microscopy (SEM)

The SEM creates a 3-D representation of the material’s surface by capturing the original shape of solid surfaces. SEM has a resolution of roughly 1 nm, which is less than TEM's. SEM can be used to characterize samples as big as 100 mm without the sample needing to be sectioned. The environmental SEM can be used to circumvent SEM's inability to characterize wet or biological samples, which is similar to TEM's limitation. The work principle of SEM is shown in Figure 3-2.

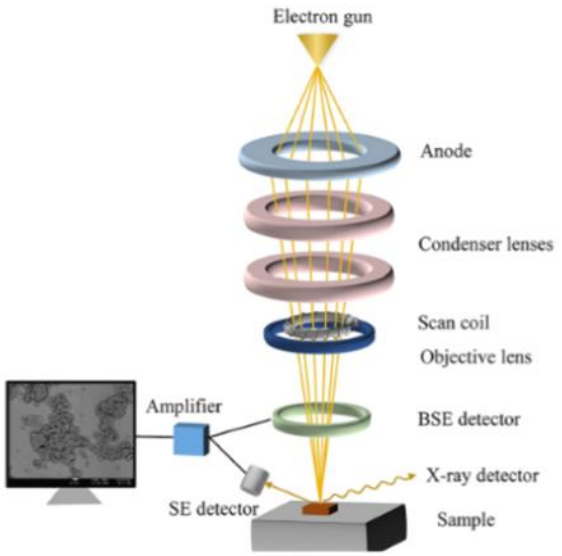

Figure 3-2. Schematic diagram of the core components of a SEM (Jian Zhao and Xia Liu, 2022).

The process begins by heating the sample at 400°C for 1 hour to remove any volatile components and ensure stability for subsequent analyses. After heating, sample undergoes thorough washing with ethanol in ultrasonic bath, repeated three to five times to remove any impurities, completely. Then, the sample is separated from the ethanol solvent via centrifugation to isolate target material. To remove any remaining solvent, separated sample is vacuum dried in oven at 60°C overnight, promoting evaporation of the ethanol and ensuring sample's purity. After sample preparation, laboratory resource reservation is managed through scheduling platform for efficient use of facilities. Upon arrival at lab, NCs are prepared for imaging procedures. 10 nm gold surface is selected, and a small piece of double-sided tape is attached onto it. NCs are carefully placed onto tape, and surface assembly is cleaned using gas in specialized cleaner. After cleaning, the sample is analyzed by using the electron microscopy. This imaging technique allows detailed examination of sample's morphology and structure, enhancing understanding of its properties and potential applications.

3.3 Performance evaluation of the nano-inhibitor

Following characterization of the NC, the focus turns to analysis tools of the nano-inhibitor's efficacy level evaluation. UV-visible spectrophotometer was used to determine absorbance value for asphaltene onset point (AOP) shifting observation, to build calibration curve of adsorption isotherm models, and to determine absorbance of the supernatant liquid of the TGA samples. TGA was used to evaluate thermogravimetric stability and behavior to extreme heat. In this section, stages of completion for each experimental investigations and interpretation tools of the raw analytical data are outlined.

3.3.1 UV-vis spectroscopy for AOP determination

The physical method used to investigate optical spectroscopy is UV-vis spectroscopy, also referred to as ultraviolet-visible spectroscopy. To examine the characteristics of molecules and materials, it makes use of light that exists in the apparent ultraviolet and near-infrared regions. The Beer-Lambert law, which states that the amount of radiation absorbed of a solution is proportional to the amount of the substance that absorbs and the route length, serves as the cornerstone of UV-vis spectroscopy. Detection of impurities, structural clarification of naturally occurring substances,

qualitative and quantitative analysis, chemical analysis, estimation of constants for dissociation of bases and acids, determination of molecular weights and investigation of deviations from Beer-Lambert law are all common applications of the technique. Sample preparation stages for AOP determination with UV-vis spectrophotometer is shown in Figure 3-3.

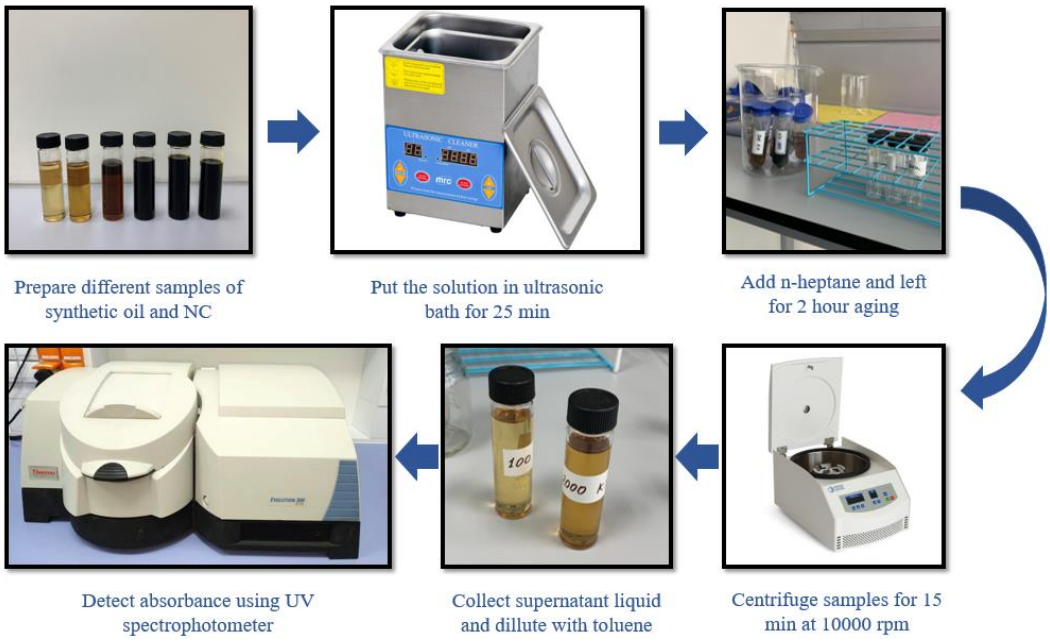

Figure 3-3. Sample preparation for AOP determination.

UV-vis spectroscopy sample preparation starts with preparing different samples of synthetic crude oil and NC. The solution is then put in ultrasonic bath for 25 min. Then *n*-heptane is added and left for aging. The samples are centrifuged for 15 min at 10,000 rpm. The supernatant liquid is then collected and diluted with toluene. Absorbance using UV-vis spectroscopy is detected.

The method uses spectrophotometry to assess the near ultraviolet (200–400 nm) absorbing of pure color by colorless substances. By the study of the absorption of ultraviolet power, that stimulates electron from their neutral state to the initial singlet excited state, the absorbance spectrum of substances in suspension or as solids are determined. The Beer-Lambert law, as expressed by:

$$A = \varepsilon l c \qquad \text{Eq. 3-2}$$

where ε is the molar absorption coefficient ($Lmol^{-1}cm^{-1}$), which describes the interaction between incident radiation and asphaltene molecules, and l is the cell thickness (cm), and c is the asphaltene concentration (mol/L). It has been verified that for both converted and unconverted asphaltenes in a dilution range, the change in intensity with quantity of asphaltene in toluene was exactly linear. The measurement precision of 0.015, which is expected to be the same for every experiment, was determined by repeating the identical adsorption experiment four times (Marchal et al., 2010).

The solutions were diluted with toluene to the required absorbance value for high asphaltene concentrations (> 250 mg/L), and the actual concentration was calculated through the multiplication of the resulting concentration by the factor of dilution (Mullins, 1998). Using the mass balance in the following equation, quantity of the adsorbed asphaltenes has been determined:

$$Q = \frac{C_o - C_e}{A} V \qquad \text{Eq. 3-3}$$

where V is volume of the solution in L, dry surface area of the NC designated as A in m^2, C_0 is the initial concentration of asphaltenes in solution (mg/L), and C_e is the equilibrium concentration of asphaltenes in the supernatant liquid (mg/L).

3.3.2 Thermogravimetric analysis (TGA)

Composition of NC and virgin asphaltene, the impact of additives, and the assessment of oxidative and catalytic effects, and thermal stability can all be determined using the temperature fluctuations in weight acquired by the TGA method. This approach can be used to analyze mass loss due to oxidation, degradation that often yields a temperature versus mass plot.

The kinetic parameters were determined from the thermogravimetric curves using the Broido method. The activation energy of the NC is estimated using plots of ln(ln(1/Y)) vs 1000/T for various stages of thermal decomposition, where Y represents the proportion not yet decomposed (Broido, 1969). TGA measures the mass of a NC as a function of temperature when the material being investigated is placed under a temperature software that is monitored in a controlled setting (Earnest, 1988). Concentration of the samples used for adsorption experiments are shown in Table 3-1. Sample preparation stages for TGA analysis and adsorption isotherm determination with UV-vis spectrophotometer is shown in Figure 3-4.

Table 3-1. Concentration of the samples used for adsorption experiments (UV-vis spectroscopy and TGA).

Adsorption experiments range	Added NP concentration	Reference
from 300 to 3,000 mg/L	10g/L	T. Wang et al., 2022
between 100 and 30,000 mg/L	100 mg per 10 mL	Cortés et al., 2016
100−3,000 mg/L	5g/L	Hosseinpour et al., 2013

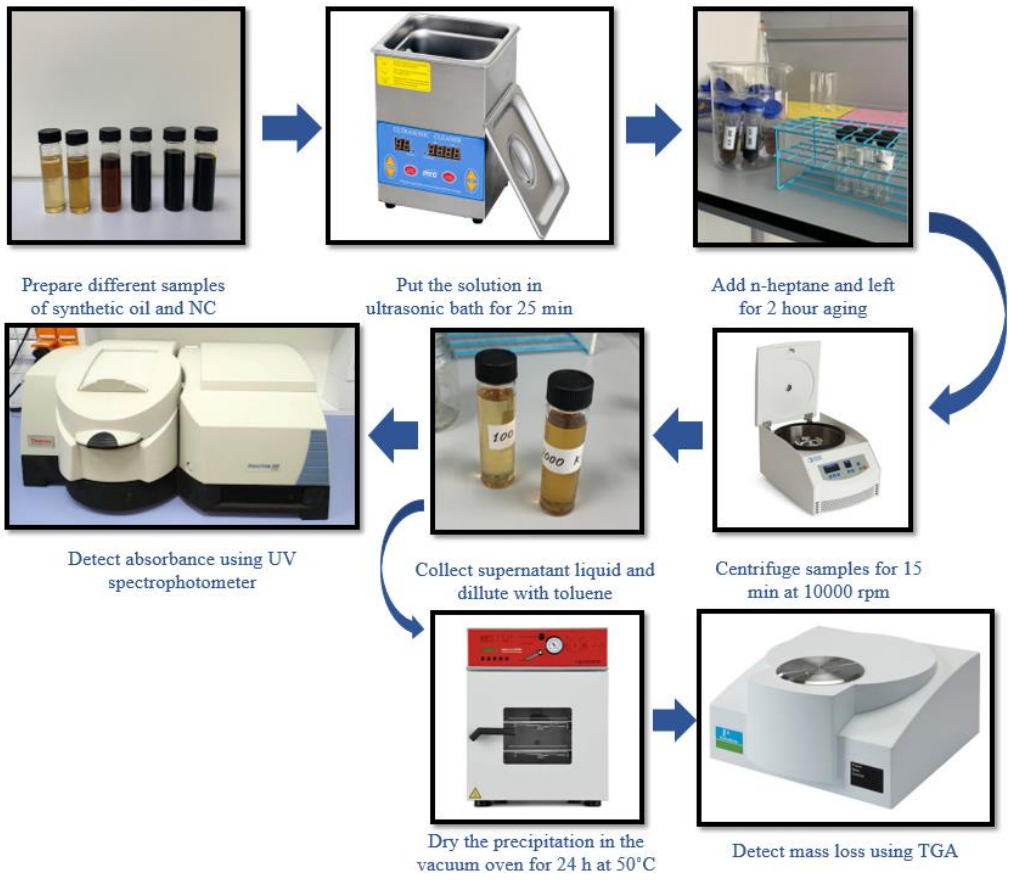

Figure 3-4. Sample preparation for TGA analysis and adsorption isotherm determination.

Different batches of synthetic crude oil, toluene, and NC were carefully prepared as mentioned in the Table 3-2 to ensure consistency across the experiments. After this preparation, solution undergoes ultrasonic treatment for 25 minutes to ensure thorough mixing of the components. Following ultrasonic treatment, solution is agitated in shaker for 24 hours at 300 revolutions per minute (rpm) to promote interaction between the constituents and achieve optimal reaction kinetics. After agitation, samples are centrifuged at 10,000 rpm for 15 minutes to separate the components based on density.

Table 3-2. Volume calculation of the TGA samples.

C of solution, ppm	**C of solution, wt%**	**V of solution, ml**	**V of toluene, ml**
100	0.01	0.6	29.4
200	0.02	1.2	28.8
400	0.04	2.4	27.6
1000	0.1	6.0	24.0
2000	0.2	12.0	18.0
5000	0.5	30.0	0.0

The resulting supernatant liquid and precipitated materials are then separated to enable further analysis of the NC. Supernatant liquid after centrifugation of the TGA samples is illustrated in Figure 3-5. The precipitated materials are dried in vacuum oven at 50°C for 24 hours to remove any remaining solvent and ensure purity of the NC. TGA analysis is conducted on dried precipitate to assess thermal stability and decomposition behavior. This analysis helps to determine suitability of the NC for various applications. Six samples with varying concentrations were prepared for TGA analysis.

Figure 3-5. Supernatant liquid after centrifugation of TGA samples.

4 RESULTS AND DISCUSSION

The results obtained from conducting the designed experiments to achieve the research objectives described in Chapter 1, are presented and discussed in detail in this chapter. First part, NC characterizations analytical tests conducted by using XRD, SEM, FTIR, TGA, and BET are presented and discussed. Various properties of the NC including its surface area, functional groups, surface morphology, particle size, crystallite size, and thermal stability are determined. To evaluate efficacy of the novel nano-inhibitor for adsorption, oxidation, and inhibition of asphaltene particles from synthetic crude oil medium using two main approaches of TGA analysis and UV-vis spectroscopy conducted in both absence and presence of the NC as described in detail in Chapter 3. UV-vis spectroscopy was used for AOP determination and study of adsorption kinetics of the asphaltene and construction of adsorption isotherm models. A discussion of mechanisms of asphaltene inhibition by using the novel nano-inhibitor is presented. At the end, a brief comparative discussion of performance of different NC-based nano-inhibitors with the nano-inhibitor developed and tested in this research work is presented.

4.1 NC characterization

The focus of this section is on detailed examination of features and characteristics of the NC. A comprehensive analysis using TGA, BET, FTIR, DLS, XRD, and SEM results is conducted. Each technique acts as a complementary tool to examine and explain various features and properties of the NC that is the basis of the nano-inhibitor for asphaltene adsorption and inhibition.

4.1.1 Thermogravimetric analysis (TGA)

TGA analysis of the SiO_2-KCl-Xanthan NC is presented in Figure 4-1. Simultaneous Thermal Analyzer (STA) 6000 was used for TGA analysis that records the changes in mass of the sample as temperature rises steadily. It enables assessment of the sample's thermal stability and presence of volatile components. The y-axis displays the mass loss percentage; while, the x-axis displays the temperature in °C. At the start of the test and prior to heating or deterioration, the sample's initial mass is 100%. The sample gets heated between 30°C and 800°C at a rate of 10°C/min. The NC sample had a base mass of 18.188 mg. The SiO_2-KCl-Xanthan NC exhibited a three stage mass loss as shown in Figure 4-1. Sudden changes in the slope of the mass loss curve indicates abrupt changes in the rate of mass loss. These can correspond to either phase transitions or chemical

reactions. The TGA curve for SiO_2-KCl-Xanthan NC showed that NC degradation occurs at approximately 230°C. As the temperature rose, the rate of mass loss increased, as well. Under 180°C, there was a 5% mass loss, which was caused by desorption of water. At 310°C, almost 33% of the mass was lost; after that, the rate of mass loss decreased and only revealed a one-step degrading process (Banerjee et al., 2006). Under 80°C, there was only a 0.4% mass loss caused by water desorption. At 800°C, the mass loss was around 50%. These findings demonstrate the first peak of the mass loss rate indicates the valuable property of temperature resistance in NCs. Evaporation of the volatile components at about 90°C. The dihydroxylation of organic material and separation of water in the material's structure are identified by the second component of mass loss rate that occurs at 290°C. Temperatures above 330°C, which suggest loss of the structural water, are associated with the latter stage of mass loss (Nazarahari et al., 2021).

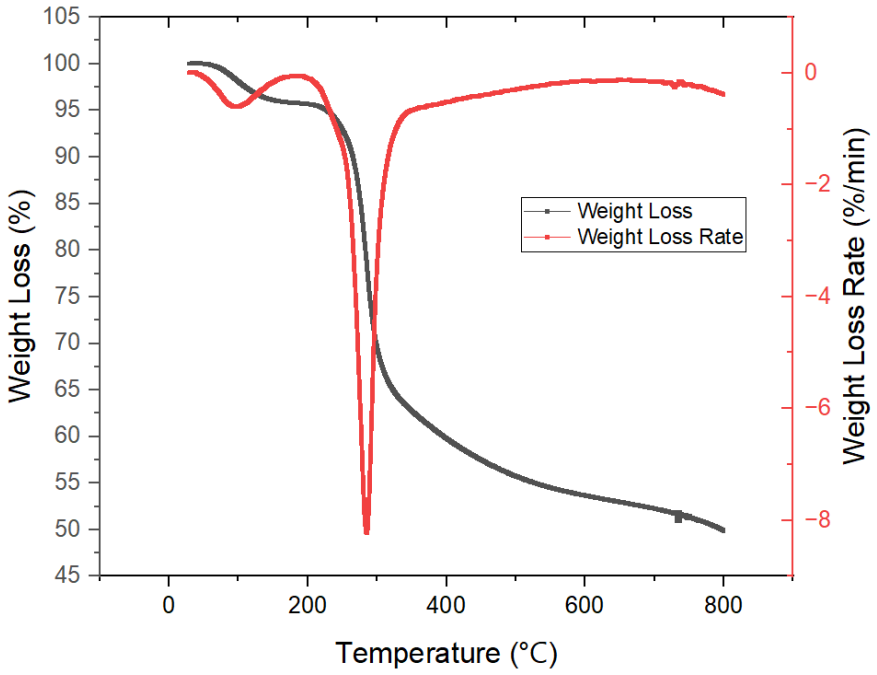

Figure 4-1. TGA analysis of the SiO_2-KCl-Xanthan NC showing the mass loss and mass loss rate during heating.

4.1.2 Brunauer-Emmett-Teller (BET) measurement

The Brunauer−Emmet−Teller (BET) equation was used to determine the surface area of the sample uing the BET data. The total pore volume was calculated by N_2 uptake at relative pressure P/P_O = 0.99 using Barrett−Joyner−Halenda (BJH) method. The chemical and physical adsorption of

nitrogen gas onto the surface of the solid material underpins the BET technique by Nitrogen porosimeter. When characterizing the NP/NC, measuring the surface area is a crucial parameter. Because the adsorption process highly depends on surface area of NPs/NCs. BET measurement is the best method to find specific surface area, directly. BET Surface Area of the NC is 31.95 m^2/g as shown in Figure 4-2. The total pore volume is equal to 0.299 cc/g.

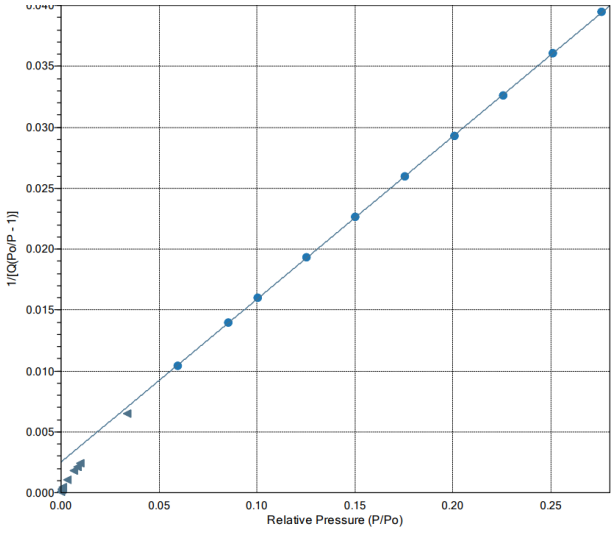

Figure 4-2. The BET tests results sued to determine the specific surface area of the SiO_2-KCl-Xanthan NC.

The isotherm linear plot of the SiO_2-KCl-Xanthan NC is shown in Figure 4-3 that shows as type V adsorption where pores fill up as the relative pressure increases.

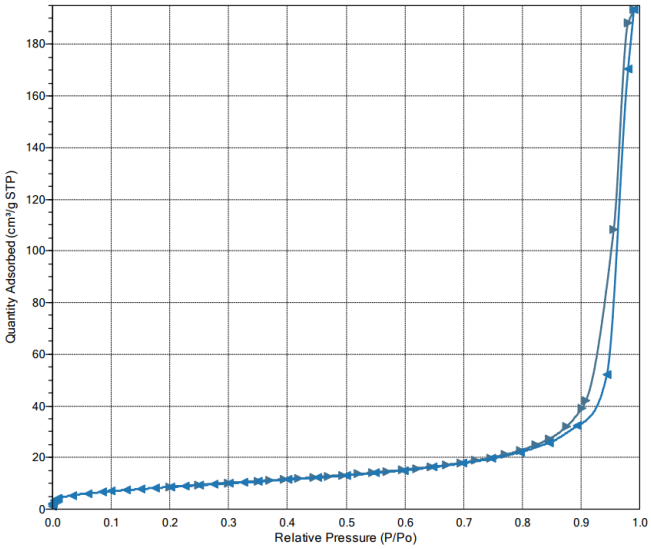

Figure 4-3. Isotherm of the SiO_2-KCl-Xanthan NC obtained from the BET analysis.

4.1.3 DLS

A Nanoparticle Tracking Analysis Instrument (PMX-230 ZetaView TWIN Laser) system operating at a temperature of 25°C with disposable microcuvettes and with a wavelength of 488 nm was used for DLS measurement. The device is able to measure the zeta-potential and analyze the particle size using Doppler electrophoresis and dynamic light scattering.

The SiO_2-KCl-Xanthan NC's size distribution versus relative number of NC particles is displayed in Figure 4-4. Particle diameter functions are used to display the contributions in terms of Number. Even with fluctuations, the particle scatter analysis revealed the particle size ranges from 30 to 300 nm, which is consistent with the SEM observations (next section). Thus, it is evident that the NC particles are hydrodynamically disrupted in size. However, as no surfactant was used to stabilize the NC, the DLS data indicated a higher particle size than the crystallite size determined by using XRD data. This is of agglomeration and clustering of the nanofluid.

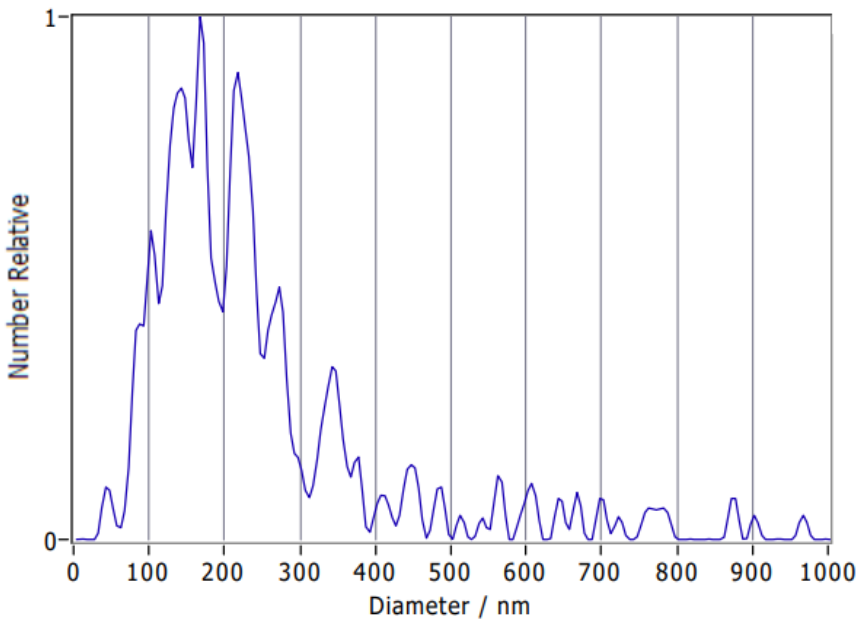

Figure 4-4. Size distribution of the SiO_2-KCl-Xanthan NC.

4.1.4 SEM

The NC particle size and surface morphology was analyzed using the Scanning Electron Microscope ZEISS Crossbeam 540 apparatus. The SEM images taken from the NC are shown in Figures 4-8. The NC's structure appears as aggregates of rounded particles exhibiting a vague, soft, and airy texture. The SiO_2 and KCl NPs are evenly dispersed across the xanthan substrate's

surface. The NC's homogeneous, spherical structure and particle size in the nanoscale range are demonstrated by SEM micrographs, indicating the effective synthesis of NCs. The xanthan's polygonal polymer matrix and the connections between its polymer structures are also visible in the SEM pictures. The average size of particles was determined between 30 nm and higher. The majority of NC grains are clustered, posing a challenge in way of accurately determining their diameter and surface structure.

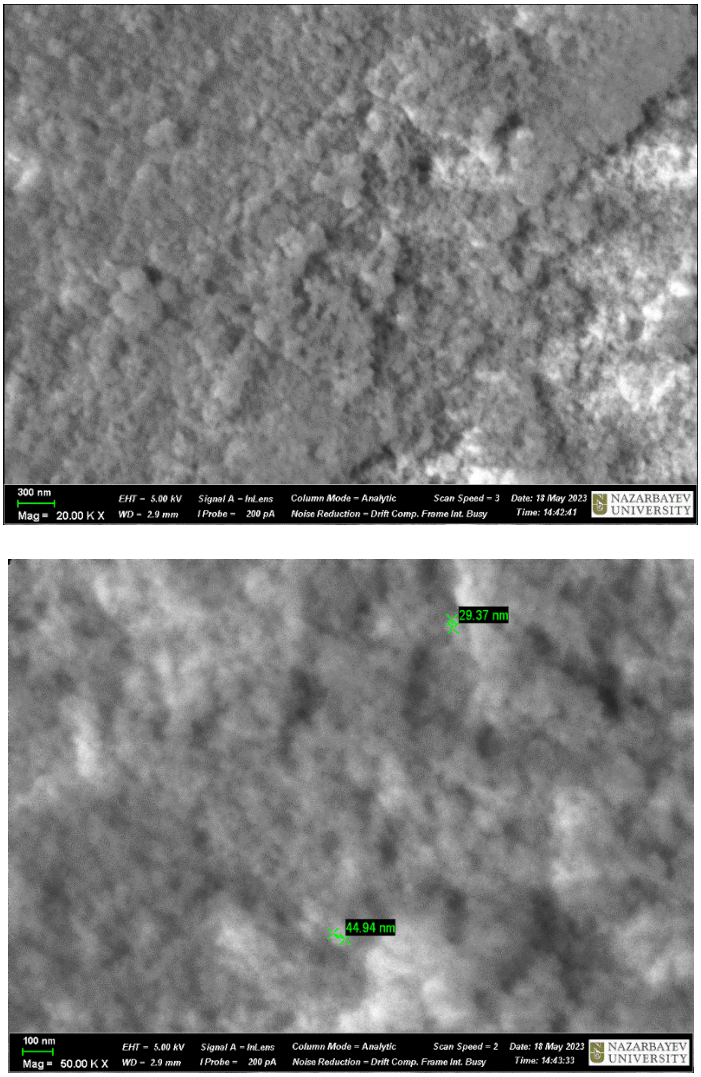

Figure 4-5. SEM images of the SiO_2-KCl-Xanthan NC NC a) 300 nm scale b) 100 nm scale.

4.1.5 XRD

The XRD analysis of the NC was conducted using SmartLab Rigaku X-ray Diffraction System. The analytical raw data of XRD was exported to asc data file for matching and fitting the peaks. The XRD pattern of the NC is shown in Figure 4-6. Three primary peaks indicate the presence of SiO_2 and KCl in the synthesized NC. The absence of any diffraction peak from other contaminants in the XRD pattern indicates that the NC has a high phase purity. The XRD pattern generally features a characteristic broad peak that is connected to the amorphous phase SiO_2 and displays the associated small particles and their inner structure, indicating high purity. (Motraghi et al., 2023). From the SiO_2-KCl-Xanthan NC's XRD pattern, the first diffraction peak of SiO_2 is centered on 20° (2θ) was visibly very broad, and absence of other reflections confirms its amorphous nature (Sun et al., 2017). In addition, the peak at 28° (2θ) is related to the SiO_2. For the KCl, the XRD pattern shows two peaks at 40.54° and 66.4° (2θ). The highest peak located at 20.15° which is 0.351 radian. According to the Scherrer's equation, the NC crystallite size is 41 nm at this peak.

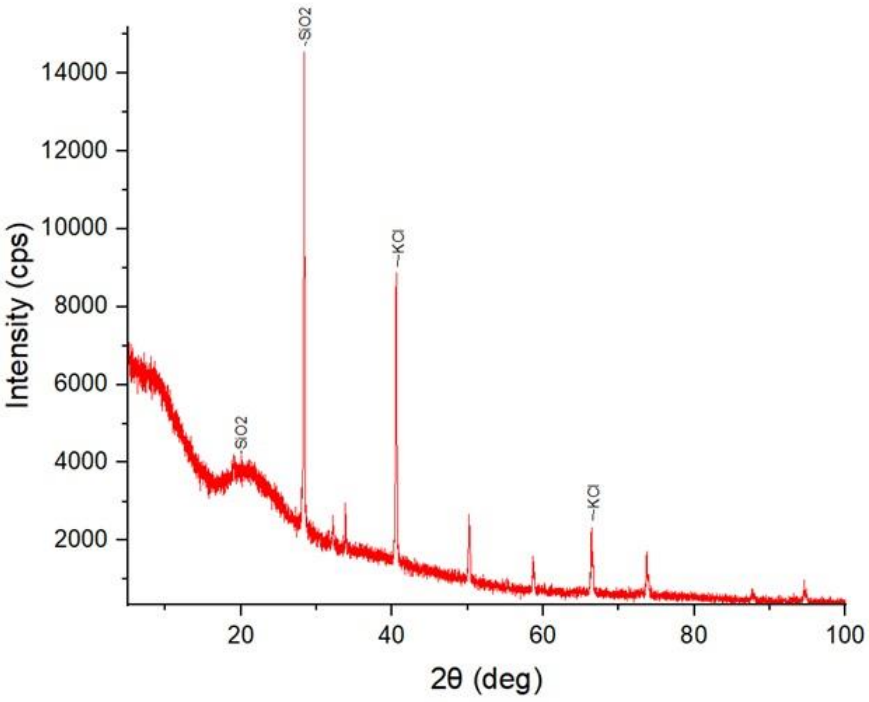

Figure 4-6. XRD analysis of the SiO_2-KCl-Xanthan NC.

4.1.6 FTIR

The FTIR analysis of the NC was conducted using a Nicolet iS10 FTIR Spectrometer at 400–4,000 cm^{-1} wavelength range. FTIR spectra can provide information on chemical bonds in the NC under infrared radiation. The FTIR spectra of the SiO_2-KCl-Xanthan NC is presented in Figure 4-10. Atomic vibrations brought on by infrared radiation may be reflected in various transmission energy peaks. Stretching vibrations O-H are responsible for the peak for xanthan polymer at 3278 cm^{-1} (Pal et al., 2012). Stretching vibrations of the COO^- group are attributed to the peak at 1604 cm^{-1} (Mittal et al., 2015; Thakur et al., 2016). According to Thakur et al. (2017), there is a peak around 1050 cm^{-1} that corresponds to the acetyl group. The peak of 1050 cm^{-1} for SiO_2 NPs is ascribed to the Si-O-Si stretching. Bending vibration of Si-OH-Si was found at 803 cm^{-1}. Peaks 1050, 803, and 444 cm^{-1} in the spectrum suggest that SiO_2-KCl-Xanthan NC is formed. According to Motraghi et al. (2023), the principal peaks at around 450, 800, 1,050, 1,600, and 3,300 cm^{-1} are associated with C–C, stretching C=O, stretching C–O, sp3-stretched C–H, and stretching O–H bonds, respectively. Based on the aforementioned spectrum, presence of organic functional groups of phytochemicals adsorbed on NC's surface suggests that the NC was properly synthesized. Additionally, the removal of some xanthan peaks with SiO_2-KCl-Xanthan NC suggests that xanthan had a role in SiO_2 NPs' creation process (Al-Yasiri et al., 2019).

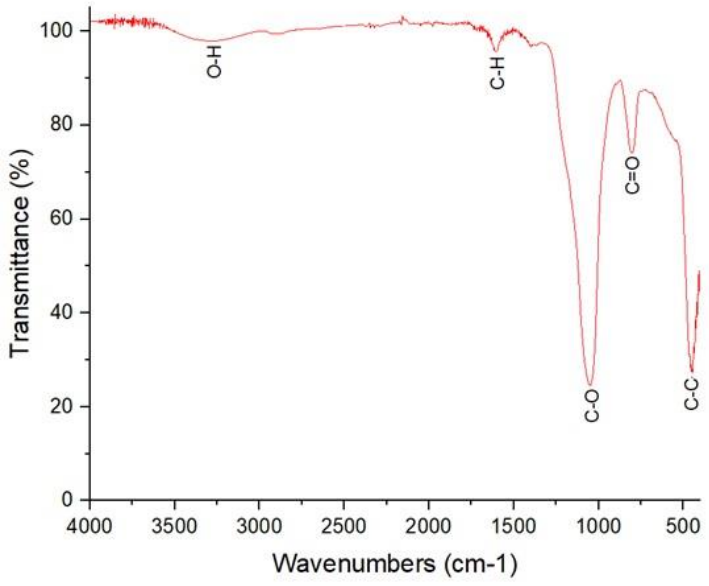

Figure 4-7. The FTIR spectra of the SiO_2-KCl-Xanthan NC.

4.2 Efficiency evaluation of the SiO_2-KCl-Xanthan nano-inhibitor

The results obtained for the determination of AOP applying TGA analysis and UV-vis spectroscopy are discussed in this section. The latter was used for AOP determination and adsorption kinetics modeling of the process of asphaltene adsorption onto the NC

4.2.1 AOP shifting by adsorption

The onset point curves of asphaltene were constructed with and without the NC at a certain concentration. The onset point in the absence of the NC must first be identified to late evaluate the effect of SiO_2-KCl-Xanthan NC on asphaltene precipitation. The absorbance versus *n*-heptane content (from 10 to 90 vol%) in the prepared synthetic crude oil samples containing 0.5 wt% asphaltene is shown in Figure 4-8. As the amount of *n*-heptane in the mixture increases, the absorbance value drops as the asphaltene concentration lowers. The absorbance and concentration are directly proportional, according to the Beer-Lambert law. Up to 40 vol%, there is a linear association in the data and adherence to Beer-Lambert's rule as seen in Figure 4-8. Nonetheless, a departure from the linear pattern is observed at 40 to 50 vol% *n*-heptane. Because of this abrupt decrease in absorbance, the linear trend is invalid throughout this concentration range. It can be inferred that asphaltene precipitates at a rate of 40 to 50 vol% *n*-heptane, which lowers the absorbance. Consequently, the beginning of asphaltene precipitation is indicated by a departure from linear. Following this, the solution's asphaltene absorbance value abruptly decreases, greatly lowering the asphaltene concentration. To properly identify the difference between the starting point and the precise percentage of *n*-heptane necessary for the precipitation's onset, three midpoints were chosen from the intervals above. Precipitation contents at these midpoints were 43, 45, and 48 vol%, in that order. According to Figure 4-10, the asphaltene onset point without NC corresponds to 40% of the *n*-heptane volume.

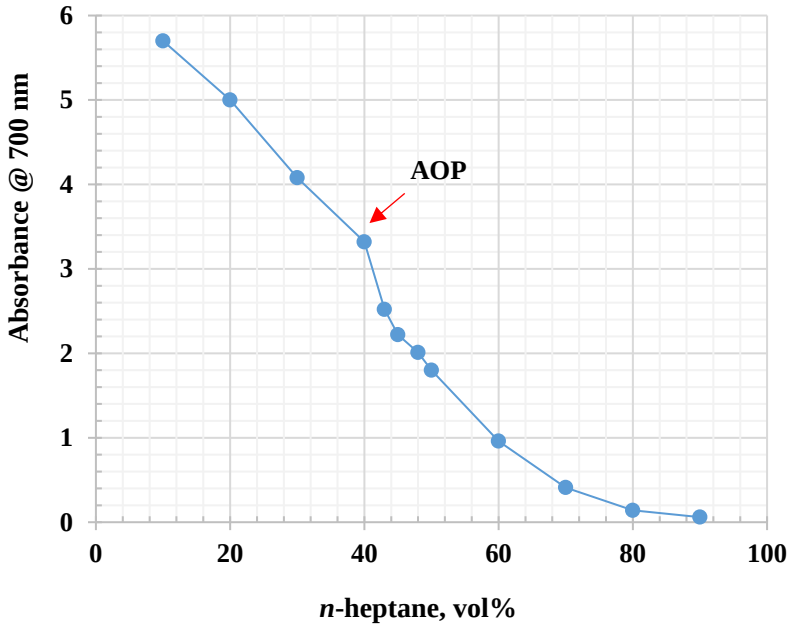

Figure 4-8. AOP determination for synthetic crude oil with 0.5 wt% asphaltene, 10–90 vol% *n*-heptane, and without the NC.

Once the onset point for the synthetic oil was determined, the impact of presence of NC with different concentrations on precipitation of asphaltene in several synthetic crude oil samples was investigated. To examine the inhibitory effect of the SiO_2-KCl-Xanthan NC on the onset point of the synthetic crude oils containing 0.5 wt% asphaltene, four SiO_2-KCl-Xanthan NC concentrations (0.1, 0.2, 0.3, and 0.4 wt%) were used. Before adjusting for the dilution effect, Figures 4-9 to 4-12 show the absorbance as a function of *n*-heptane concentration to establish the synthetic crude oil's onset point in both presence and absence of the SiO_2-KCl-Xanthan NC.

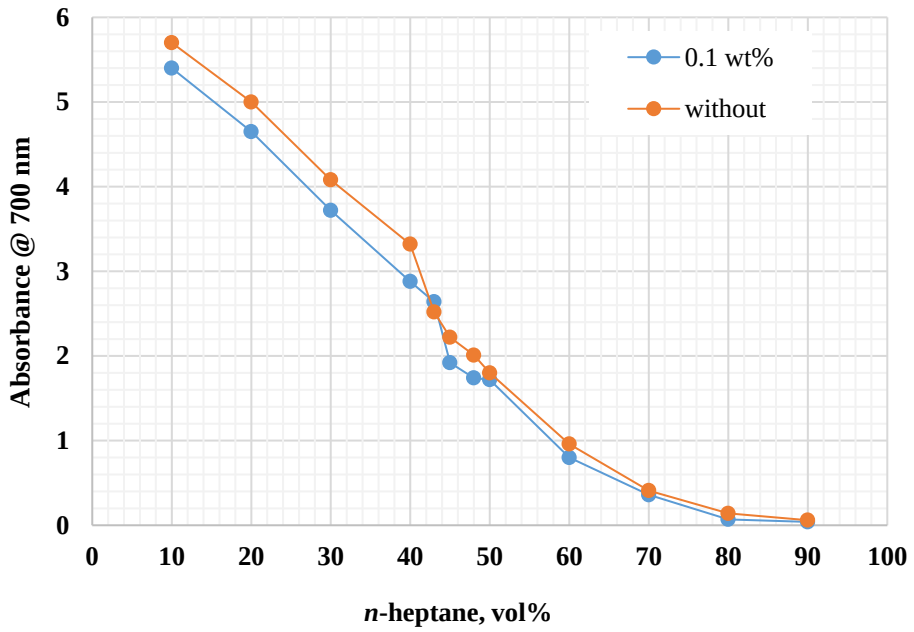

Figure 4-9. AOP determination for synthetic crude oil with 0.5 wt% asphaltene, 10–90 vol% *n*-heptane, and 0.1 wt% NC.

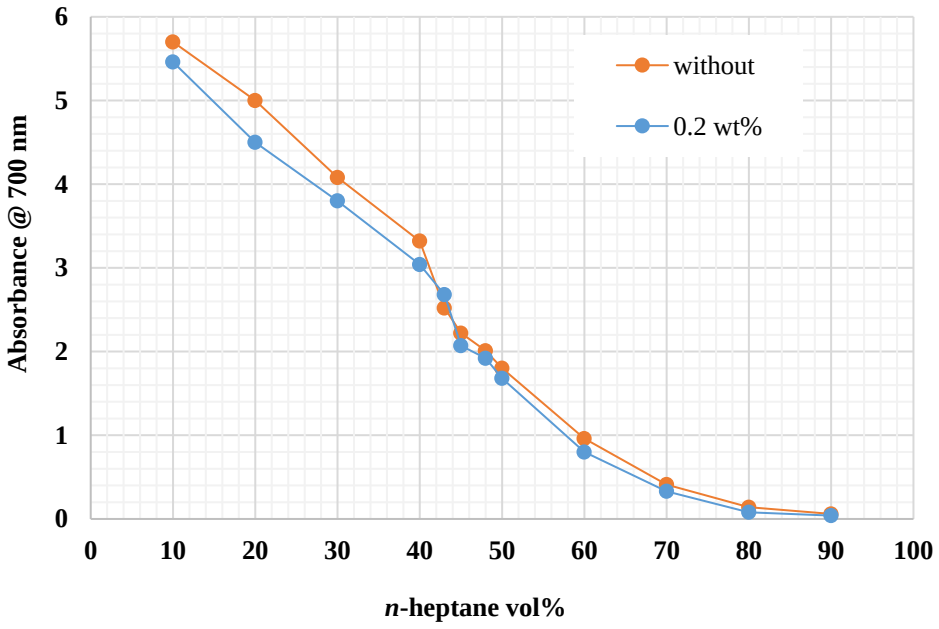

Figure 4-10. AOP determination for synthetic crude oil with 0.5 wt% asphaltene, 10–90 vol% *n*-heptane, and 0.2 wt% NC.

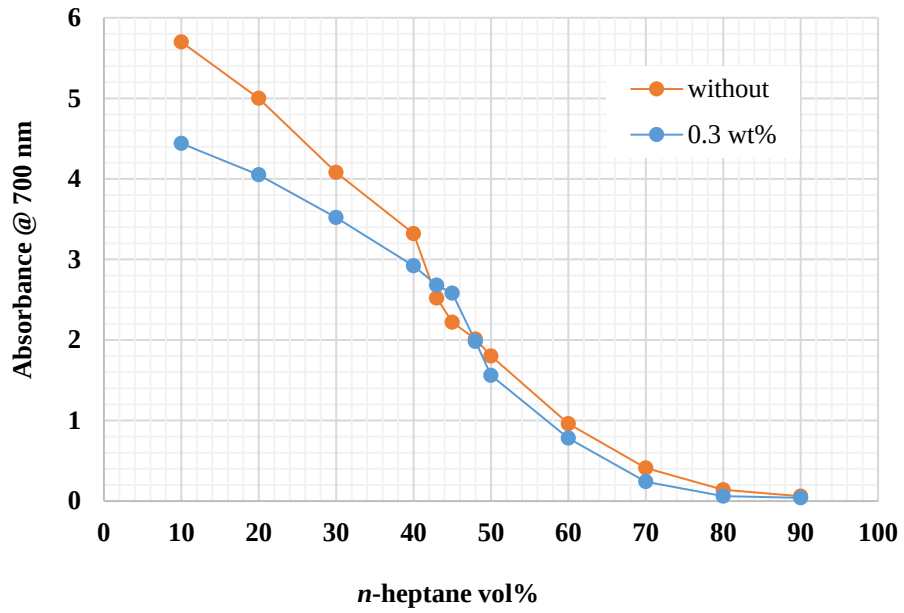

Figure 4-11. AOP determination for synthetic crude oil with 0.5 wt% asphaltene, 10–90 vol% *n*-heptane, and 0.3 wt% NC.

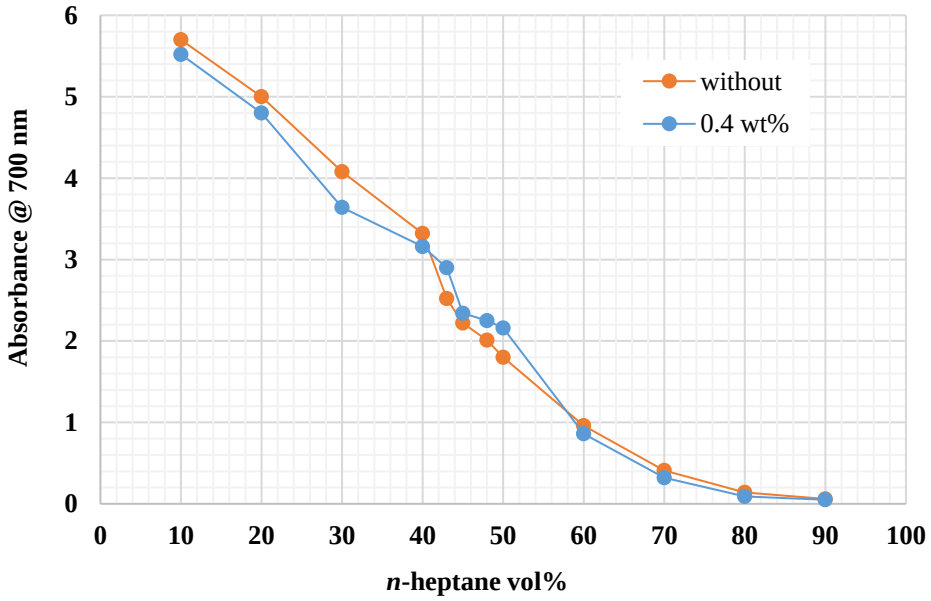

Figure 4-12. AOP determination for synthetic crude oil with 0.5 wt% asphaltene, 10–90 vol% *n*-heptane, and 0.4 wt% NC.

It is evident from Figure 4-13 that the addition of SiO_2-KCl-Xanthan NC has delayed the onset point of asphaltene precipitation. The amount of asphaltenes in the synthetic crude oil is reduced and the AOP is shifted and delayed by eliminating the adsorbed asphaltenes that were separated during centrifugation. As depicted in Figure 4-13, the AOP shifts to 43, 43, 45, and 43 vol% *n*-heptane when 0.1, 0.2, 0.3, and 0.4 wt% SiO_2-KCl-Xanthan NC is used, respectively. The AOP values determined for synthetic crude oil with 0.5 wt% asphaltene concentration and various concentrations of the NC are shown in Table 4-1. The optimum NC concentration that is the best AOP shifting concentration was 0.3 wt% of NC. At this concentration, the AOP is shifted from 40 vol% to 45 vol% and then decreased to 43 vol% at 0.4 wt% of NC concentration.

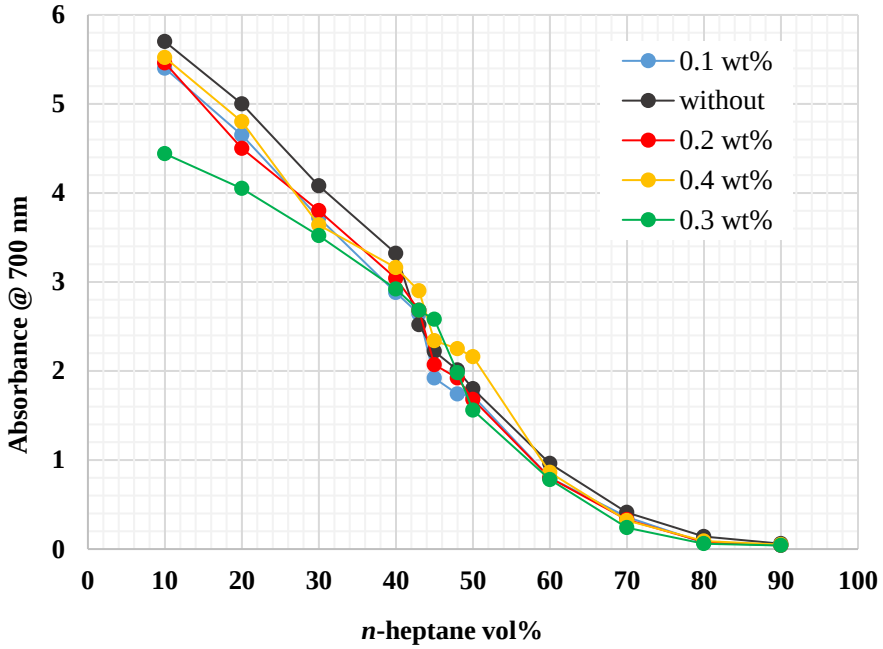

Figure 4-13. AOP determination for synthetic crude oil with 0.5 wt% asphaltene, 10–90 vol% *n*-heptane, and different concentrations of the NC.

Table 4-1. AOP values determined for synthetic crude oil with 0.5 wt% asphaltene concentration and various concentrations of the NC

NC concentration, wt%	0	0.1	0.2	0.3	0.4
AOP by *n*-heptane, vol%	40	43	43	45	43

4.2.2 TGA analysis

Thermogravimetric analysis enables determining the level of asphaltene adsorption onto surface of the SiO_2-KCl-Xanthan NC. The difference in behavior and degree of oxidation and combustion by raising the temperature of the environment to 800°C is observed. The TGA data was used to evaluate thermal degradation and oxidation processes by measuring mass loss as it changed with temperature. The TGA technique was used to examine asphaltene concentrations 100, 200, 400, 1000, 2000 and 5,000 ppm. The experimental samples have been heated in the Thermal Analyzer with temperature condition from 30°C to 800°C at a rate of 10°C/min. Mass loss profiles provides investigations on the decomposition and oxidation processes. Figure 4-14 depicts the mass loss from pure or virgin asphaltene. Mass loss happened in two stages. The first step of mass loss at temperatures ranging from 150°C to 350°C was allocated to the water and liquids evaporation from the asphaltene sample, as well as the decomposition of the asphaltene molecules. The second stage of the mass loss process occurred between 400°C and 800°C as a result of burn and loss of organic chains of the asphaltene after the decomposition and oxidation process. The absence of plateau behavoir in the last part of the mass loss line suggests that the pure asphaltene sample did not burn completely.

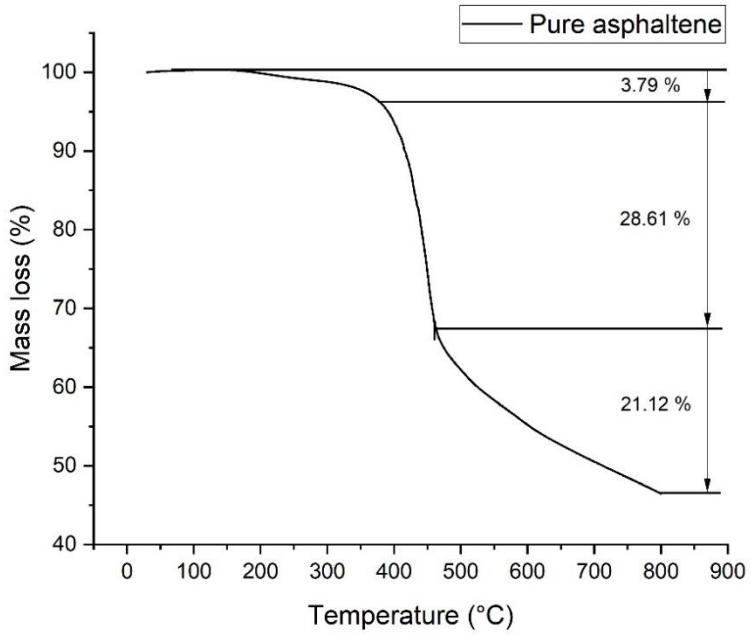

Figure 4-14. Pure asphaltene mass loss.

Mass loss of adsorbed asphaltene molecules onto the nanocomposite surface with 2000 ppm concentration occurred in two stages (Figure 4-15). The first starts from 80°C to 200°C and the second continues with 220°C until 500°C. Adsorbed asphaltene was completely burnt and oxidized because of the increased surface area exposed to the NC.

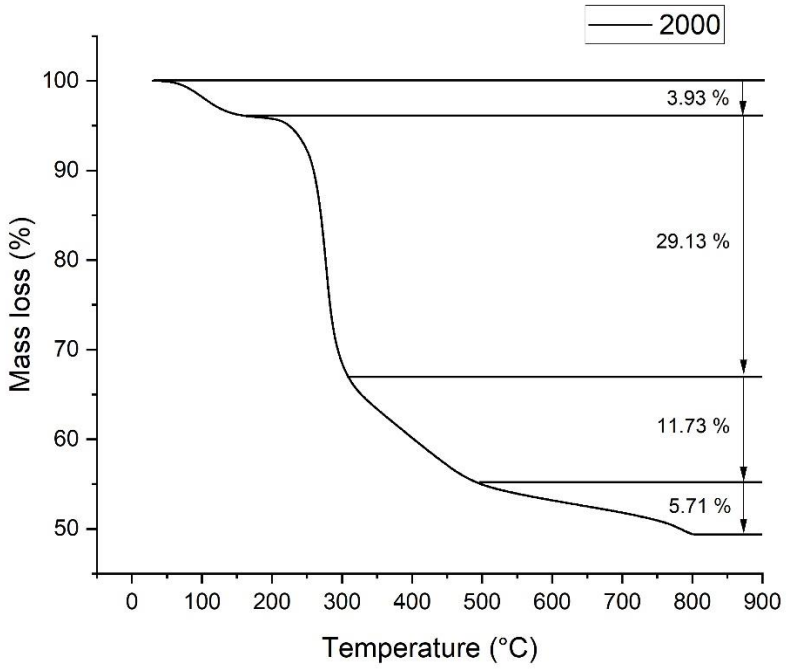

Figure 4-15. The mass loss of 2000 ppm asphaltene concentration sample adsorbed onto SiO_2-KCl-Xanthan NC.

53% of the synthetic crude oil and the virgin or pure asphaltene was burnt as shown in Figure 4-16. In samples containing NC, this value was reduced to 50%. The asphaltene line highlights two stages of mass degradation. The first episode began at 350°C and continued to decline beyond 470°C. The second stage began at 470°C and continued to drop until the end of the experiment at 800°C.

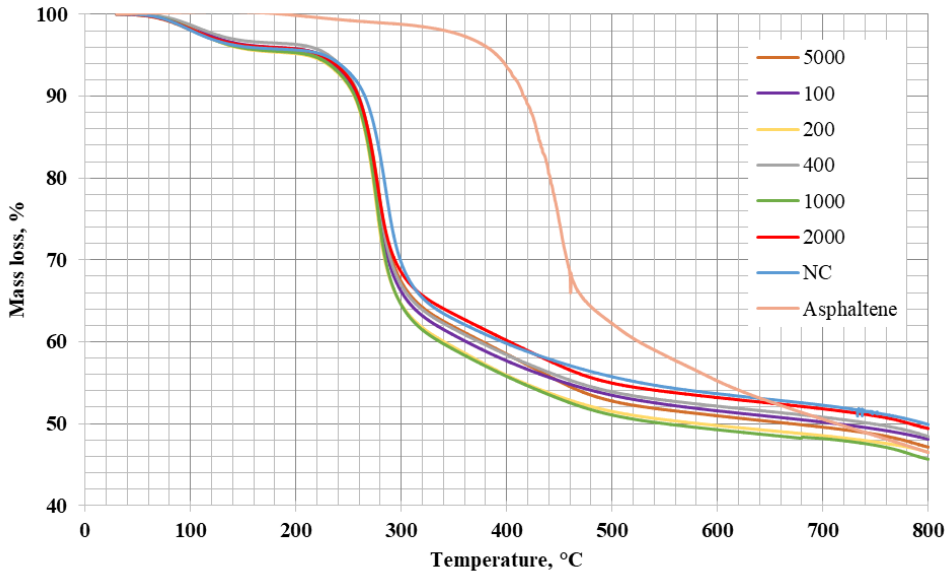

Figure 4-16. Weight loss of the pure asphaltene and SiO_2-KCl-Xanthan NC and adsorbed asphaltene with concentrations of NC, 100 to 5,000 ppm obtained from TGA analysis.

The function of the NC in increasing asphaltene oxidation was revealed by the thermos-oxidative profiles from TGA analysis. The fractional conversion, α, can be calculated using Eq. 4-1:

$$\alpha = \frac{m_0 - m_t}{m_0 - m_\infty} \qquad \text{Eq. 4-1}$$

where m_0 is initial mass of the sample, m_∞ is final mass of the sample, and m_t is mass of sample at any time. In principle, fractional conversion, α, should provide an intensive variable for evaluation of condensed phase reaction kinetic parameters. A plot of α against temperature for the NC at varying asphaltene uptake values is presented in Figure 4-17. Understanding the mass loss and oxidation process of the adsorbed asphaltene requires a knowledge of the fraction conversion. Mass is not a factor in this variable. The lines finally meet at temperatures between 250°C and 300°C as they converge. The TGA curves are in increasing order from low to higher concentrations of adsorbed asphaltene samples followed by pure or virgin asphaltene. The NC exhibited a catalytic function. This confirms the similar observations reported in the literature by Abu Tarboush & Husein (2012) and Arstanova (2023). Oxidation of virgin asphaltene started at around 400-450℃; while oxidation of 5,000 ppm sample with NC started at around 280℃. The NC has

catalyzed oxidation of the asphaltene. This thermo-oxidative profile indicates catalytic function of the NC that is attributed to affinity of adsorption asphaltene onto the NC.

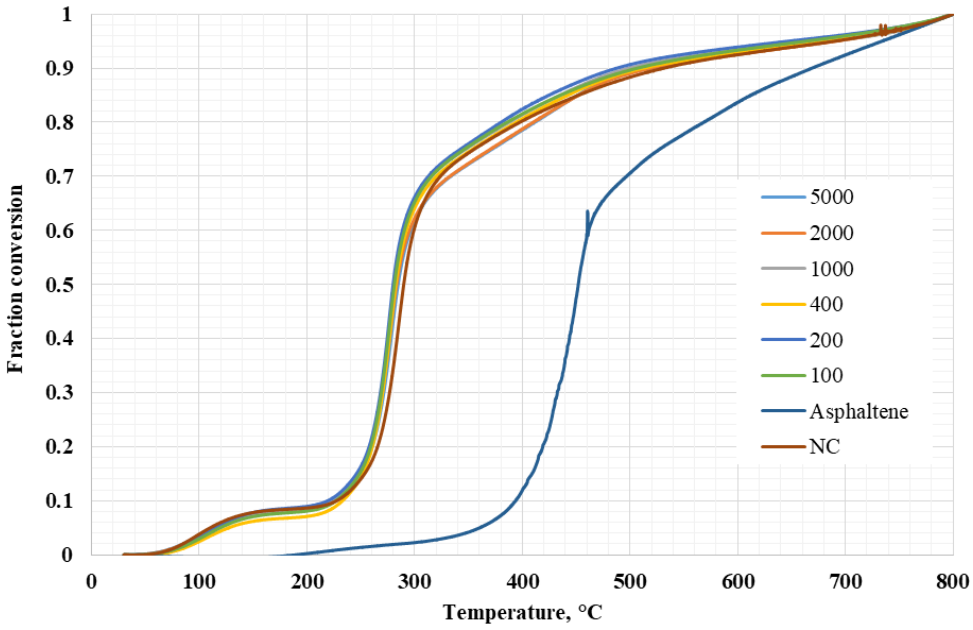

Figure 4-17. Conversion factor of pure asphaltene, SiO_2-KCl-Xanthan NC, and the adsorbed asphaltene onto NC with NC concentrations.

4.2.3 Asphaltene adsorption kinetics isotherm modeling

As outlined previously in the TGA analysis section, the TGA tests were done using the adsorbed asphaltene onto NC with NC concentrations of 100, 200, 400, 1000, 2000, and 5000 ppm. The supernatant from TGA analysis was used for adsorption kinetics isotherm modeling. The calibration curve is shown in Figure 4-16 was constructed at a wavelength of 700 nm using UV-vis spectroscopy measurements. It adheres to Beer-Lambert's law's linear function, which is frequently used to measure an object's absorbance in order to calculate its concentration in solution. The calibration curve shown in 4-16 exhibits an indirect proportionality between the concentration and absorbance. The graph's linear equation was used to compute the equilibrium concentration, which was required for precise adsorption kinetics isotherms modeling.

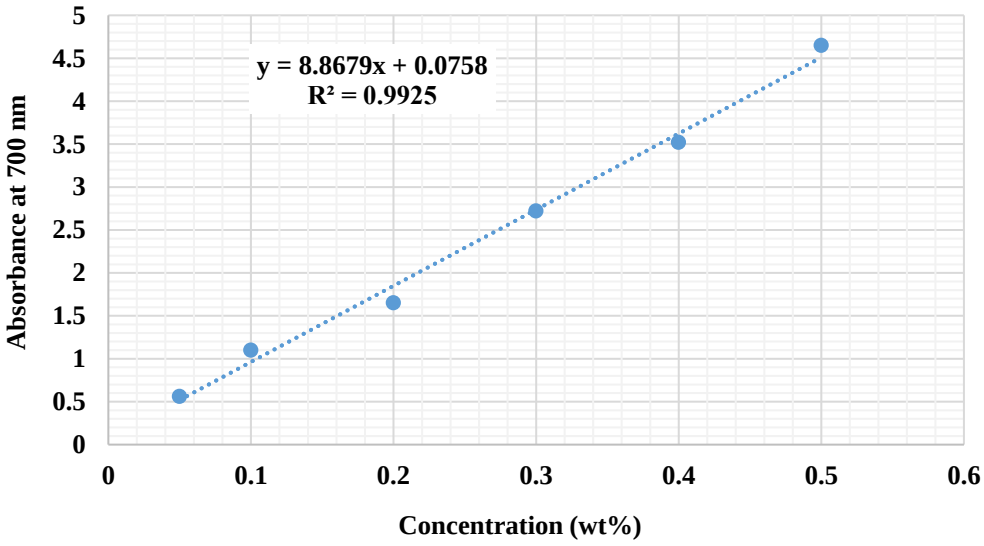

Figure 4-18. Calibration curve for asphaltene without NC.

Adsorption kinetics isotherm modeling is used to generate mathematical models that can effectively predict the adsorption parameters of asphaltene adsorption onto the NC. The relationship that exists between the concentration of dispersed adsorption material in the liquid at equilibrium and the amount of adsorbents adsorbed on the adsorbent is described by an adsorption isotherm. The quantity of asphaltene adsorbed per unit weight of the adsorbent is denoted by parameter Q_{eq}, and the rest of the asphaltene concentration in the solution is indicated by the value C_{eq}.

Equation of Langmuir isotherm model:

$$\frac{C_{eq}}{Q_{eq}} = \frac{1}{bQ_m} + \frac{C_{eq}}{Q_m} \qquad \text{Eq. 4-2}$$

where b is constant isotherm Langmuir, Q_m is the capacity for adsorption.

Equation of Freundlich isotherm model:

$$\log Q_{eq} = \log K + \frac{1}{n}\log C_{eq} \qquad \text{Eq. 4-3}$$

where n and *K* are the Freundlich constants, Q_e is adsorbent quantity, C_e is the material's concentration is not adsorbent.

The concentration of supernatant liquid was calculated using Equation 4-4.

$$C_1V_1 = C_2(V_1 + V_2) \qquad \text{Eq. 4-4}$$

where C_1 is initial concentration, C_2 is diluted concentration, V_1 is the volume of crude oil with different concentrations, V_2 is volume of toluene used for dilution. The initial absorbance value was calculated using Equation 4-5.

$$\frac{A_d}{C_d} = \frac{A_i}{C_i} \quad \text{Eq. 4-5}$$

The equilibrium concentration of asphaltene was calculated using Equation 4-6.

$$C_e = C_0 - \frac{m}{V} \quad \text{Eq. 4-6}$$

where C_0 is initial concentration of asphaltene in the solution, m is mass of the absorbent (depicted as mass of the NC in the solution), and V is volume of the solution.

The Langmuir and Freundlich isotherm models constructed in this research work are presented in Figures 4-17 to 4-19. The models' parameters that show the maximum amount of asphaltene adsorbed onto NC's surface, Q_{max}; the Langmuir constant, K_L; Freundlich adsorption constant, K_F and adsorption intensity factor, 1/n; and R^2 coefficients are shown in Table 4-1.

Table 4-1. Langmuir and Freundlich isotherm models' parameters obtained for the adsorption of asphaltene onto SiO_2-KCl-Xanthan NC.

Isotherm models	**Langmuir**			**Freundlich**		
Parameters	$Q_m\left(\frac{mg}{m^2}\right)$	$K_L\ (\frac{L}{mg})$	R^2	$K_F(\frac{mg}{g})(\frac{1}{g})^{\frac{1}{n}}$	1/n	R^2
25˚C	1.33	0.018	0.98	17.23	0.13	0.82

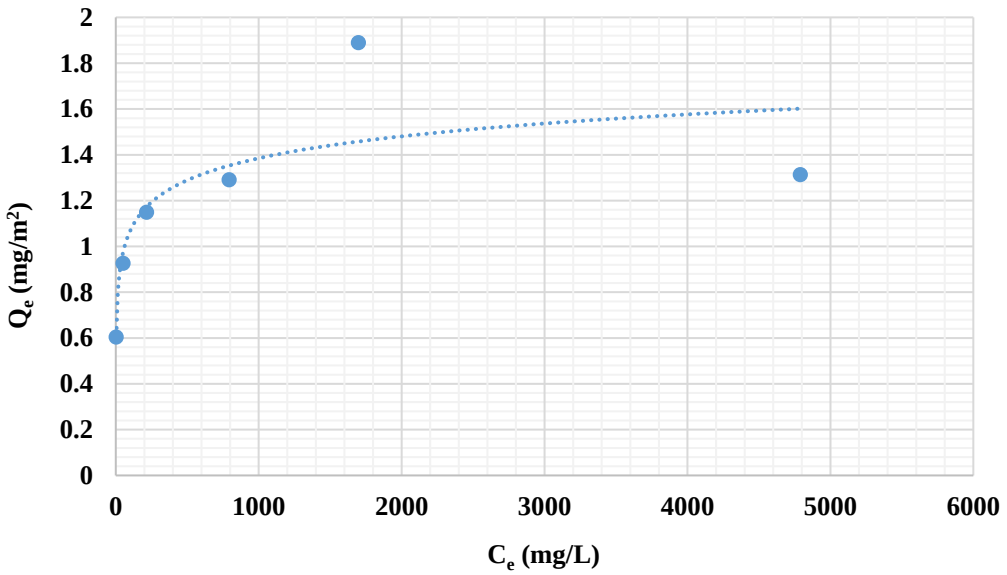

Figure 4-19. Adsorption isotherm results. The data points are the experimental data.

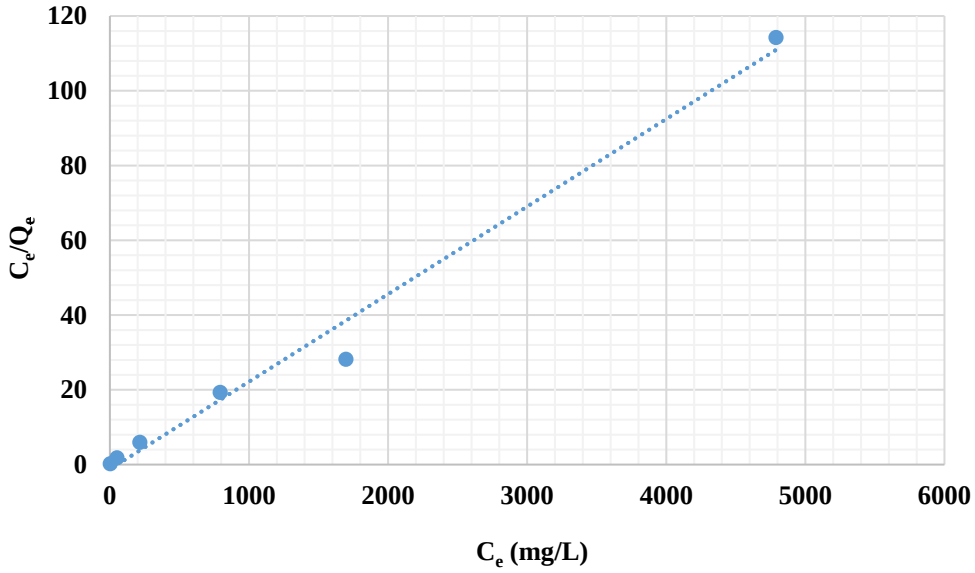

Figure 4-20. Langmuir isotherm model of adsorption of asphaltene onto SiO2-KCl-Xanthan NC. The data points are the experimental data.

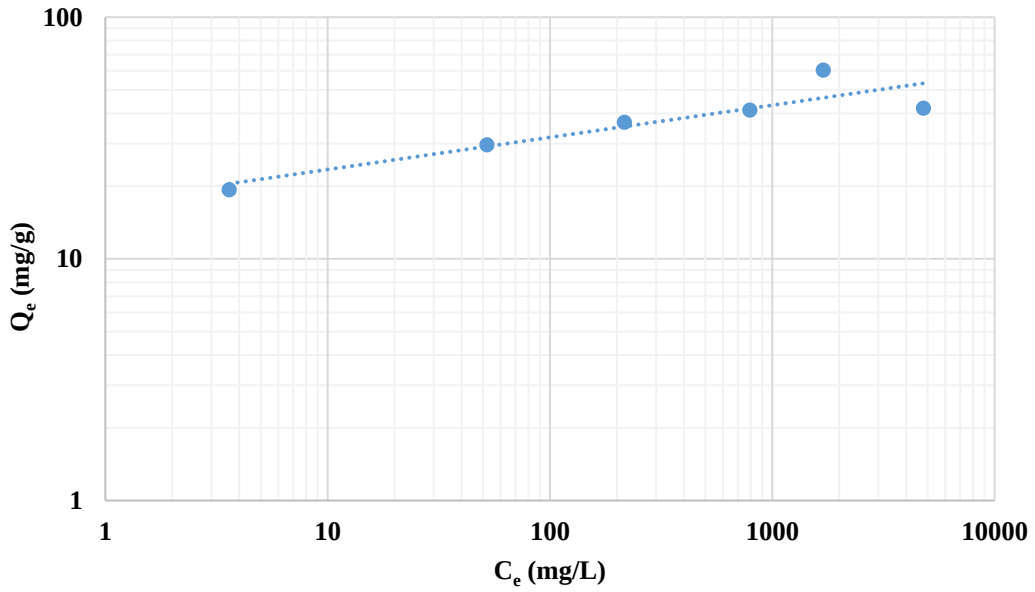

Figure 4-21. Freundlich isotherm model of adsorption of asphaltene onto SiO_2-KCl-Xanthan NC. The data points are the experimental data.

The outcome of asphaltene adsorption kinetics isotherm modeling suggests that the Langmuir adsorption isotherm model with R^2 value of 0.98 fits the experimental data better than the Freundlich adsorption isotherm model R^2 of 0.82 indicating a monolayer asphaltene adsorption onto the surface of SiO_2-KCl-Xanthan NC. Langmuir model presupposes monolayer adsorption, where the adsorbed layer has a thickness of one molecule. Additionally, it makes the assumption that there are only a limited number of distinct, equivalent, confined locations where adsorption can take place and that there are neither steric nor lateral interactions between the molecules (Foo & Hameed, 2010).

4.3 Comparison with previously reported research works

In this section, an attempt was made to compare performance of the SiO_2-KCl- Xanthan nano-inhibitor with three other novel NCs. This is contrary to the fact that a direct comparison is not feasible even if the same asphaltene is used to test the inhibitors, as there are still several differences between both NCs such as particle size, surface area, chemistry, and other parameters that have an impact on asphaltene adsorption capacity. Arstanova (2023) developed and tested a novel CuO-SiO_2-Montmorillonite-K^+-Thiazine inhibitor. Ten (2023) developed and tested a novel Thiazine-Fe_3O_4-TiO_2-SiO_2-Bentonite inhibitor. Both performed well under laboratory conditions.

Serikbay (2024) also developed and tested a NiO-Fe_3O_4-Polythiophene inhibitor with promising results. The asphaltene used by Serikbay (2024) is same as this present research work that enables a better comparison between the two nano-inhibitors. A summary of properties of the NCs and their inhibitory efficiency is presented in Table 4-2. The NiO-Fe_3O_4-Polythiophene inhibitor is superior to the SiO_2-KCl-Xanthan inhibitor despite the fact that the crystallite size is twice bigger. The inhibitor is also more thermally stable and supports both mono and multilayer deposition.

Table 4-2. Comparison between performance parameter of different nano-inhibitors.

Researcher	**Crystallite size, XRD, nm**	**size range, SEM, nm**	**Surface area, (m^2/g)**	**Optimum NC concentration, wt%**	**AOP shift, %**	**Mass loss at 800˚C, %**	**Langmuir model's R^2**	**Freundlich model's R^2**
CuO-SiO_2-Montmorillionite-K^+-Thiazine (Arstanova, 2023)	70.7	83-257	46.427	0.3	7	12.3	0.98	0.97
Thiazine-Fe_3O_4-TiO_2-SiO_2-Bentonite (Ten, 2023)	46	60-240	43.84	0.3	7	10	0.99	0.84
Polythiophene-NiO-Fe_3O_4 Serikbay (2024)	33.2	60-400	55.8	0.3	8	21.3	0.98	0.95
Present research work: SiO_2-KCl-Xanthan (Kaliolla, 2024)	41	30-300	31.95	0.3	5	50	0.98	0.82

Particle size of the NCs widely varies and ranges from 29 to 413 nm as identified by SEM images. However, the size of crystallite ranges from 33.2 to 70.7 nm. BET measurements shows highest surface area of about 55.8 m^2/g obtained for NiO-Fe_3O_4-Polythiophene. The SiO_2-KCl-Xanthan NC undergo rapid decay of under high temperature due to presence of xanthan natural polymer. All experiments ended up with highest shifting of AOP at a 0.3 wt% concentration of

NC added to the synthetic oil with 0.5 wt% of asphaltene concentration. This consistency shows that the results are reliable across different charaterization values. The Langmuir and Freundlich adsorption isotherm models fitted well in all inhibitors. Langmuir adsorption isotherm with R^2 of 0.98 compared with the Freundlich model with R^2 values of 0.82 to 0.84 support a monolayer asphaltene adsorption deposition model. The exception was Arstanova (2023) and Serikbay (2024)'s works where both models fitted well concluding both mono and multilayer adsorption occurrence. This research works demonstrated promising efficiency for novel nano-inhibitors for asphaltene adsorption and precipitation prevention at laboratory conditions that might be applied in the field in future.

5 CONCLUSIONS AND RECOMMENDATIONS

Based on extensive experimental investigations conducted in this research work, performance of SiO_2-KCl-Xanthan NC as an asphaltene precipitation inhibitor for adsorption of asphaltene from a synthetic crude oil medium was thoroughly evaluated. The asphaltene was extracted from a heavy crude oil obtained from a west Kazakhstani oilfield using the IP-143 standard. Analytical techniques including SEM, FTIR, BET, XRD, DLS, and TGA were sued to first to characterize surface morphology and particle size, to determine functional groups and elemental bonding, to determine surface area, to estimate crystallite and size structure, to obtain particle size distribution, and to measure thermal stability of the NC, respectively. In the next step, efficacy of the nano-inhibitor in mitigating asphaltene precipitation inhibition was assessed using AOP shift determination and asphaltene adsorption kinetics isotherm modeling using UV-vis spectroscopy and supernatant obtained from TGA analysis. The following conclusions can be drawn from this experimental research work:

1. Through SEM analysis, it was determined that the NC has a particle size ranging from 29 nm to 44 nm, with the crystallite size of 41 nm was obtained using XRD results. The NC's homogeneous, spherical structure and particle size in the nanoscale range are demonstrated by SEM micrographs, indicating the effective synthesis of the NC. BET measurement indicated surface area of 31.95 m^2/g, highlighting the NC's potential for effective adsorption. The particle is primarily 30 to 300 nm in size from DLS measurement.
2. The NC exhibited high adsorptive capacity and effectively inhibited asphaltene precipitation. Specifically, the Asphaltene Onset Point (AOP) was shifted from 40% to 45% *n*-heptane volume ratio at an optimal concentration of 0.3 wt% NC, indicating a significant improvement in inhibitory performance.
3. TGA analysis revealed the NC's ability to promote asphaltene oxidation at lower temperatures. This reduction in oxidation temperature suggests enhanced asphaltene adsorption onto the NC, leading to improved oxidation efficiency.
4. Adsorption isotherm analysis indicated that the adsorption of asphaltene onto the NC followed dominantly the Langmuir model, suggesting the occurrence of both monolayer and multilayer adsorption processes.

Based on these conclusions, some recommendations for further investigation are proposed:

- Further explore the performance of individual nanoparticles (NPs) in inhibiting asphaltene precipitation to understand their respective contributions compared to the complex NC. Additionally, compare the performance of other NCs under similar conditions to assess their effectiveness in different asphaltene samples.
- Investigate the performance of the NC under simulated reservoir conditions to better understand its efficacy in real-world applications.
- Continuously optimize the synthesis process of the NC to enhance its performance and versatility in mitigating asphaltene-related challenges.
- Explore the catalytic impact of the NC on promoting other reactions, such as pyrolysis and gasification, to uncover additional applications beyond asphaltene inhibition.

REFERENCES

Adams, J. J. (2014). Asphaltene adsorption, a literature review. Energy & Fuels, 28(5), 2831-2856.

Adebiyi, F. M. (2021). An insight into asphaltene precipitation, deposition and management stratagems in petroleum industry. Journal of Pipeline Science and Engineering, 1(4), 419-427.

Ahmadi, A., Manshad, A. K., Ali, J. A., Iglauer, S., Sajadi, S. M., Keshavarz, A., & Mohammadi, A. H. (2022). Insight into nano-chemical enhanced oil recovery from carbonate reservoirs using environmentally friendly nanomaterials. ACS omega, 7(41), 36165-36174.

Ahmadi, Y., & Aminshahidy, B. (2018). Effects of hydrophobic CaO and SiO2 nanoparticles on Asphaltene Precipitation Envelope (APE): An experimental and modeling approach. Oil & Gas Science and Technology–Revue d'IFP Energies nouvelles, 73, 56.

Ahmed, M. A., Abdul-Majeed, G. H., & Alhuraishawy, A. K. (2023). An integrated review on asphaltene: definition, chemical composition, properties, and methods for determining onset precipitation. SPE Production & Operations, 38(02), 215-242.

Akbarzadeh, K., Hammami, A., Kharrat, A., Zhang, D., Allenson, S., Creek, J., ... & Solbakken, T. (2007). Asphaltenes—problematic but rich in potential. Oilfield review, 19(2), 22-43.

Alboudwarej, H., Beck, J., Svrcek, W. Y., Yarranton, H. W., & Akbarzadeh, K. (2002). Sensitivity of asphaltene properties to separation techniques. Energy & Fuels, 16(2), 462-469.

Alboudwarej, H., Pole, D., Svrcek, W. Y., & Yarranton, H. W. (2005). Adsorption of asphaltenes on metals. Industrial & engineering chemistry research, 44(15), 5585-5592.

Ali, A., Cole, D. R., & Striolo, A. (2023). Understanding the aggregation of model island and archipelago asphaltene molecules near kaolinite surfaces using molecular dynamics. Energy & Fuels, 37(16), 11662-11674.

Alimohammadi, S., Zendehboudi, S., & James, L. (2019). A comprehensive review of asphaltene deposition in petroleum reservoirs: Theory, challenges, and tips. Fuel, 252, 753-791.

Al-Qasim, A., Al-Anazi, A., Omar, A. B., & Ghamdi, M. (2018, November). Asphaltene precipitation: a review on remediation techniques and prevention strategies. In Abu Dhabi International Petroleum Exhibition and Conference (p. D021S046R001). SPE.

Al-Yasiri, M., Awad, A., Pervaiz, S., & Wen, D. (2019). Influence of silica nanoparticles on the functionality of water-based drilling fluids. Journal of Petroleum Science and Engineering, 179, 504-512.

Andersen, S. I., & Christensen, S. D. (2000). The critical micelle concentration of asphaltenes as measured by calorimetry. Energy & Fuels, 14(1), 38-42.

Ansari, S., Bahmaninia, H., Mohammadi, M. R., Ostadhassan, M., Norouzi-Apourvari, S., Schaffie, M., ... & Hemmati-Sarapardeh, A. (2022). On the evaluation of asphaltene adsorption onto dolomite surface: The roles of flow condition, composition of asphaltene, and dolomite size. Alexandria Engineering Journal, 61(12), 9411-9425.

Arsalan, N., Palayangoda, S. S., & Nguyen, Q. P. (2014). Characterization of asphaltene deposition in a stainless steel tube. Journal of Petroleum Science and Engineering, 121, 66-77.

Ashoori, S., Sharifi, M., Masoumi, M., & Salehi, M. M. (2017). The relationship between SARA fractions and crude oil stability. Egyptian Journal of Petroleum, 26(1), 209-213.

Aske, N., Kallevik, H., Johnsen, E. E., & Sjöblom, J. (2002). Asphaltene aggregation from crude oils and model systems studied by high-pressure NIR spectroscopy. Energy & Fuels, 16(5), 1287-1295.

Asomaning, S., & Watkinson, A. P. (2000). Petroleum stability and heteroatom species effects in fouling of heat exchangers by asphaltenes. Heat Transfer Engineering, 21(3), 10-16.

Asomaning, S., & Yen, A. (2002). Prediction and solution of asphaltene related problems in the field. SPECIAL PUBLICATION-ROYAL SOCIETY OF CHEMISTRY, 280, 277-286.

Banerjee, J., Srivastava, A., Srivastava, A., & Behari, K. (2006). Synthesis and characterization of xanthan gum-g-N-vinyl formamide with a potassium monopersulfate/Ag (I) system. Journal of Applied Polymer Science, 101(3), 1637-1645.

Belayneh, M., & Aadnøy, B. S. (2016, June). Effect of nano-silicon dioxide (SiO2) on polymer/salt treated bentonite drilling fluid systems. In International Conference on Offshore Mechanics and Arctic Engineering (Vol. 49996, p. V008T11A027). American Society of Mechanical Engineers.

Betancur, S., Carmona, J. C., Nassar, N. N., Franco, C. A., & Cortés, F. B. (2016). Role of particle size and surface acidity of silica gel nanoparticles in inhibition of formation damage by asphaltene in oil reservoirs. Industrial & Engineering Chemistry Research, 55(21), 6122-6132.

Broido, A. (1969). A simple, sensitive graphical method of treating thermogravimetric analysis data. Journal of Polymer Science Part A-2: Polymer Physics, 7(10), 1761-1773.

Castellon, J., Vazquez, I. R., Fréchette, M., & Fabiani, D. (2013). Nanocomposite characterization and diagnostics tools. IEEE Electrical Insulation Magazine, 29(6), 37-48.

Cortés, F. B., Mejía, J. M., Ruiz, M. A., Benjumea, P., & Riffel, D. B. (2012). Sorption of asphaltenes onto nanoparticles of nickel oxide supported on nanoparticulated silica gel. Energy & Fuels, 26(3), 1725-1730.

Cortés, F. B., Montoya, T., Acevedo, S., Nassar, N. N., & Franco, C. A. (2016). Adsorption-desorption of nc 7 asphaltenes over micro-and nanoparticles of silica and its impact on wettability alteration. CT&F-Ciencia, Tecnología y Futuro, 6(4), 89-106.

Dudášová, D., Simon, S., Hemmingsen, P. V., & Sjöblom, J. (2008). Study of asphaltenes adsorption onto different minerals and clays: Part 1. Experimental adsorption with UV depletion detection. Colloids and Surfaces A: Physicochemical and Engineering Aspects, 317(1-3), 1-9.

Earnest, C. M. (Ed.). (1988). Compositional analysis by thermogravimetry (Vol. 997). ASTM International.

Enerdata. (2022). World Energy & Climate Statistics—Yearbook 2022. World Energy Consumption Statistics, Enerdata.

Ezeonyeka, N. L., Hemmati-Sarapardeh, A., & Husein, M. M. (2018). Asphaltenes adsorption onto metal oxide nanoparticles: a critical evaluation of measurement techniques. Energy & fuels, 32(2), 2213-2223.

Fakher, S., Ahdaya, M., Elturki, M., & Imqam, A. (2020). Critical review of asphaltene properties and factors impacting its stability in crude oil. Journal of Petroleum Exploration and Production Technology, 10, 1183-1200.

Farooq, U., Patil, A., Panjwani, B., & Simonsen, G. (2021). Review on application of nanotechnology for asphaltene adsorption, crude oil demulsification, and produced water treatment. Energy & Fuels, 35(23), 19191-19210.

Foo, K. Y., & Hameed, B. H. (2010). Insights into the modeling of adsorption isotherm systems. Chemical engineering journal, 156(1), 2-10.

Franco, C. A., Montoya, T., Nassar, N. N., Pereira-Almao, P., & Cortés, F. B. (2013). Adsorption and subsequent oxidation of colombian asphaltenes onto nickel and/or palladium oxide supported on fumed silica nanoparticles. Energy & Fuels, 27(12), 7336-7347.

Franco, C. A., Nassar, N. N., Ruiz, M. A., Pereira-Almao, P., & Cortés, F. B. (2013). Nanoparticles for inhibition of asphaltenes damage: adsorption study and displacement test on porous media. Energy & Fuels, 27(6), 2899-2907.

Franco, C., Patiño, E., Benjumea, P., Ruiz, M. A., & Cortés, F. B. (2013). Kinetic and thermodynamic equilibrium of asphaltenes sorption onto nanoparticles of nickel oxide supported on nanoparticulated alumina. Fuel, 105, 408-414.

Franco-Ariza, C. A., Guzmán-Calle, J. D., & Cortés-Correa, F. B. (2016). Adsorption and catalytic oxidation of asphaltenes in fumed silica nanoparticles: Effect of the surface acidity. Dyna, 83(198), 171-179.

Freundlich, H.M.F.: J. Phys. Chem. 1906, 57,385–471.

Gharbi, K., Benyounes, K., & Khodja, M. (2017). Removal and prevention of asphaltene deposition during oil production: A literature review. Journal of Petroleum Science and Engineering, 158, 351-360.

Gray, M. R., Yarranton, H. W., Chacon-Patino, M. L., Rodgers, R. P., Bouyssiere, B., & Giusti, P. (2021). Distributed properties of asphaltene nanoaggregates in crude oils: A review. Energy & Fuels, 35(22), 18078-18103.

Guerrero-Martin, C. A., Montes-Pinzon, D., Meneses Motta da Silva, M., Montes-Paez, E., Guerrero-Martin, L. E., Salinas-Silva, R., ... & Szklo, A. (2023). Asphaltene precipitation/deposition estimation and inhibition through nanotechnology: a comprehensive review. Energies, 16(13), 4859.

Gupta, D. V. S., Szymczak, S., & Brown, M. J. (2009, January). Solid production chemicals added with the frac for scale, paraffin and asphaltene inhibition. In SPE Hydraulic Fracturing Technology Conference and Exhibition (pp. SPE-119393). SPE.

Guzmán, J. D., Betancur, S., Carrasco-Marín, F., Franco, C. A., Nassar, N. N., & Cortés, F. B. (2016). Importance of the adsorption method used for obtaining the nanoparticle dosage for asphaltene-related treatments. Energy & Fuels, 30(3), 2052-2059.

Guzmán, R., Rodríguez, S., Torres-Mancera, P., & Ancheyta, J. (2020). Evaluation of asphaltene stability of a wide range of Mexican crude oils. Energy & Fuels, 35(1), 408-418.

Hassanzadeh, M., & Abdouss, M. (2023). Molecular Structure: The First and Most Significant Factor in the Precipitation of Asphaltenes. SPE Journal, 28(02), 894-907.

Hosseini-Dastgerdi, Z., Maleki, A., Elyassi, E., & Rashidi, A. (2024). Silica/polyacrylamide nanocomposite for inhibition of asphaltene precipitation from unstable crude oils. Petroleum Science and Technology, 42(2), 250-268.

Hosseinpour, N., Khodadadi, A. A., Bahramian, A., & Mortazavi, Y. (2013). Asphaltene adsorption onto acidic/basic metal oxide nanoparticles toward in situ upgrading of reservoir oils by nanotechnology. Langmuir, 29(46), 14135-14146.

Ibrahim, H. H., & Idem, R. O. (2004). Interrelationships between asphaltene precipitation inhibitor effectiveness, asphaltenes characteristics, and precipitation behavior during n-heptane (light paraffin hydrocarbon)-induced asphaltene precipitation. Energy & Fuels, 18(4), 1038-1048.

Jamaluddin, A. K., Nazarko, T. W., & Sills, S. (1995). Asphaltene-compatible fluid design for workover operations (No. CONF-9502114-Vol. 2). UNITAR, New York, NY (United States).

Kazemzadeh, Y., Eshraghi, S. E., Kazemi, K., Sourani, S., Mehrabi, M., & Ahmadi, Y. (2015). Behavior of asphaltene adsorption onto the metal oxide nanoparticle surface and its effect on heavy oil recovery. Industrial & Engineering Chemistry Research, 54(1), 233-239.

Kelland, M. A. (2016). Production chemicals for the oil and gas industry. CRC press.

Khaksar Manshad, A., Kabipour, A., Mohammadian, E., Yan, L., A. Ali, J., Iglauer, S., ... & Moradi, S. (2023). Application of a novel green nano polymer for chemical EOR purposes in

sandstone reservoirs: Synergetic effects of different fluid/fluid and rock/fluid interacting mechanisms. ACS omega, 8(46), 43930-43954.

Kim H A; Seo J K; Kim T and Lee B T 2014 Environmental Health and Toxicology 29 1

Kong, X., & Ohadi, M. M. (2010, November). Applications of micro and nano technologies in the oil and gas industry-an overview of the recent progress. In Abu Dhabi international petroleum exhibition and conference (pp. SPE-138241). SPE.

Kuzenbayev, A. (2022). ANALYSIS OF METHODS FOR COMBATING ASPHALT-RESIN-PARAFFIN DEPOSITS IN THE FIELDS OF WESTERN KAZAKHSTAN. The Scientific Heritage, (103), 85-87.

Langmuir, I.:J. Am. Chem. Soc. 1916, 38 (11), 2221–2295.

Leyva, C., Ancheyta, J., Berrueco, C., & Millán, M. (2013). Chemical characterization of asphaltenes from various crude oils. Fuel Processing Technology, 106, 734-738.

Li, X., Guo, Y., Sun, Q., Lan, W., & Guo, X. (2018). Effect of nanoparticles on asphaltene aggregation in a microsized pore. Industrial & Engineering Chemistry Research, 57(27), 9009-9017.

Limanowka, W. A., Voytechek, M. M., & Limanowka, R. E. (1999, October). Asphaltene deposition problems in oil industry with focus on electric submersible pump applications. In SPE Annual Technical Conference and Exhibition? (pp. SPE-56662). SPE.

Linkov P; Artemyev M; Efimov A E and Nabiev I 2013 Nanoscale 5 8781

Loganathan, S., Valapa, R. B., Mishra, R. K., Pugazhenthi, G., & Thomas, S. (2017). Thermogravimetric analysis for characterization of nanomaterials. In Thermal and rheological measurement techniques for nanomaterials characterization (pp. 67-108). Elsevier.

Madhi, M., Bemani, A., Daryasafar, A., & Khosravi Nikou, M. R. (2017). Experimental and modeling studies of the effects of different nanoparticles on asphaltene adsorption. Petroleum Science and Technology, 35(3), 242-248.

Mansoori, G. A., & Soelaiman, T. F. (2005). Nanotechnology--An introduction for the standards community. ASTM International.

Maqbool, T., Raha, S., Hoepfner, M. P., & Fogler, H. S. (2011). Modeling the aggregation of asphaltene nanoaggregates in crude oil− precipitant systems. Energy & Fuels, 25(4), 1585-1596.

Marchal, C., Abdessalem, E., Tayakout-Fayolle, M., & Uzio, D. (2010). Asphaltene diffusion and adsorption in modified NiMo alumina catalysts followed by ultraviolet (UV) spectroscopy. Energy & fuels, 24(8), 4290-4300.

Marczewski, A. W., & Szymula, M. (2002). Adsorption of asphaltenes from toluene on mineral surface. Colloids and Surfaces A: Physicochemical and Engineering Aspects, 208(1-3), 259-266.

Marques, L. C., González, G., & Monteiro, J. B. (2004, September). A chemical approach to prevent asphaltenes flocculation in light crude oils: State-of-the-art. In SPE Annual Technical Conference and Exhibition? (pp. SPE-91019). SPE.

Matsushita, K., Marafi, A., Hauser, A., & Stanislaus, A. (2004). Relation between relative solubility of asphaltenes in the product oil and coke deposition in residue hydroprocessing. Fuel, 83(11-12), 1669-1674.

Mazloom, M. S., Hemmati-Sarapardeh, A., Husein, M. M., Behbahani, H. S., & Zendehboudi, S. (2020). Application of nanoparticles for asphaltenes adsorption and oxidation: A critical review of challenges and recent progress. Fuel, 279, 117763.

Mirzayi, B., & Shayan, N. N. (2014). Adsorption kinetics and catalytic oxidation of asphaltene on synthesized maghemite nanoparticles. Journal of Petroleum Science and Engineering, 121, 134-141.

Mittal, H., Maity, A., & Ray, S. S. (2015). Synthesis of co-polymer-grafted gum karaya and silica hybrid organic–inorganic hydrogel nanocomposite for the highly effective removal of methylene blue. Chemical Engineering Journal, 279, 166-179.

Mittal, V., Kim, J. K., & Pal, K. (Eds.). (2011). Recent advances in elastomeric nanocomposites (Vol. 9, p. 388). Berlin: Springer.

Mohammadi, M., Dadvar, M., & Dabir, B. (2017). TiO2/SiO2 nanofluids as novel inhibitors for the stability of asphaltene particles in crude oil: Mechanistic understanding, screening, modeling, and optimization. Journal of Molecular Liquids, 238, 326-340.

Mohammed, I., Mahmoud, M., Al Shehri, D., El-Husseiny, A., & Alade, O. (2021). Asphaltene precipitation and deposition: A critical review. Journal of Petroleum Science and Engineering, 197, 107956.

Mohammed, I., Mahmoud, M., El-Husseiny, A., Al Shehri, D., Al-Garadi, K., Kamal, M. S., & Alade, O. S. (2021). Impact of asphaltene precipitation and deposition on wettability and permeability. ACS omega, 6(31), 20091-20102.

Montes, D., Orozco, W., Taborda, E. A., Franco, C. A., & Cortés, F. B. (2019). Development of nanofluids for perdurability in viscosity reduction of extra-heavy oils. Energies, 12(6), 1068.

Motraghi, F., Manshad, A. K., Akbari, M., & Ali, J. A. (2023). Impact of Mutual Solvents on Wettability Alteration for EOR Application by Hybrid Smart Water and Green SiO2/KCl/Xanthan Nanocomposites in Carbonate Reservoirs. Energy & Fuels, 37(23), 18560-18575.

Motraghi, F., Manshad, A. K., Akbari, M., Ali, J. A., Sajadi, S. M., Iglauer, S., & Keshavarz, A. (2023). Interfacial tension reduction of hybrid crude-oil/mutual-solvent systems under the influence of water salinity, temperature and green SiO2/KCl/Xanthan nanocomposites. Fuel, 340, 127464.

Mullins, O. C. (2005, October). Molecular structure and aggregation of asphaltenes and petroleomics. In SPE Annual Technical Conference and Exhibition? (pp. SPE-95801). SPE.

Mullins, O. C. (2008). Review of the molecular structure and aggregation of asphaltenes and petroleomics. Spe Journal, 13(01), 48-57.

Mullins, O. C. (2010). The modified Yen model. Energy & Fuels, 24(4), 2179-2207.

Mullins, O. C. (2011). The asphaltenes. Annual review of analytical chemistry, 4, 393-418.

Mullins, O. C. Optical interrogation of aromatic moieties in crude oil sand asphaltenes. In Structures and dynamics of asphaltenes; Mullins, O. C.; Sheu, E. Y., Eds.; Plenum Press: New York, 1998.

Mullins, O. C., Pomerantz, A. E., Andrews, A. B., & Zuo, J. Y. (2015). Asphaltenes explained for the Nonchemist. Petrophysics, 56(03), 266-275.

Mullins, O. C., Sheu, E. Y., Hammami, A., & Marshall, A. G. (2007). Asphaltenes, heavy oils, and petroleomics. Springer Science & Business Media.

Mustapha, S., Ndamitso, M. M., Abdulkareem, A. S., Tijani, J. O., Shuaib, D. T., Mohammed, A. K., & Sumaila, A. (2019). Comparative study of crystallite size using Williamson-Hall and Debye-Scherrer plots for ZnO nanoparticles. Advances in Natural Sciences: Nanoscience and Nanotechnology, 10(4), 045013.

Nassar, N. N. (2010). Asphaltene adsorption onto alumina nanoparticles: kinetics and thermodynamic studies. Energy & Fuels, 24(8), 4116-4122.

Nassar, N. N., Betancur, S., Acevedo, S., Franco, C. A., & Cortés, F. B. (2015). Development of a population balance model to describe the influence of shear and nanoparticles on the aggregation and fragmentation of asphaltene aggregates. Industrial & Engineering Chemistry Research, 54(33), 8201-8211.

Nassar, N. N., Hassan, A., & Pereira-Almao, P. (2011). Comparative oxidation of adsorbed asphaltenes onto transition metal oxide nanoparticles. Colloids and surfaces A: Physicochemical and Engineering aspects, 384(1-3), 145-149.

Nassar, N. N., Hassan, A., & Pereira-Almao, P. (2011). Metal oxide nanoparticles for asphaltene adsorption and oxidation. Energy & Fuels, 25(3), 1017-1023.

Nassar, N. N., Husein, M. M., & Pereira-Almao, P. (2011). In-situ prepared nanoparticles in support of oilsands industry meeting future environmental challenges. Explor. Prod. Oil Gas Rev, 9(1), 46-48.

National Nanotechnology Initiative. (2015). National Science and Technology Council. Committee on Technology, Subcommittee on Nanoscale Science, National Technology Initiative Strategic Plan.

Nazarahari, M. J., Manshad, A. K., Ali, M., Ali, J. A., Shafiei, A., Sajadi, S. M., ... & Keshavarz, A. (2021). Impact of a novel biosynthesized nanocomposite (SiO2@ Montmorilant@ Xanthan) on wettability shift and interfacial tension: Applications for enhanced oil recovery. Fuel, 298, 120773.

Ngata, M. R., Yang, B., Aminu, M. D., Iddphonce, R., Omari, A., Shaame, M., ... & Yanyi-Akofur, D. (2021). Review of Developments in Nanotechnology Application for Formation Damage Control. Energy & Fuels, 36(1), 80-97.

Oh, K., & Deo, M. D. (2002). Effect of organic additives on the onset of asphaltene precipitation. Energy & fuels, 16(3), 694-699.

Oschmann, H. J. (2002). New methods for the selection of asphaltene inhibitors in the field. Special publication-royal society of chemistry, 280, 254-263.

Pal, S., Ghorai, S., Das, C., Samrat, S., Ghosh, A., & Panda, A. B. (2012). Carboxymethyl tamarind-g-poly (acrylamide)/silica: a high performance hybrid nanocomposite for adsorption of methylene blue dye. Industrial & Engineering Chemistry Research, 51(48), 15546-15556.

R. Parsaei, Y. Kazemzadeh, M. Riazi, Study of Asphaltene Precipitation during CO2 Injection into Oil Reservoirs in the Presence of Iron Oxide Nanoparticles by Interfacial Tension and Bond Number Measurements, ACS Omega 5 (14) (2020) 7877–7884

Ratulowski, J., Amin, A., Hammami, A., Muhammad, M., & Riding, M. (2004, September). Flow assurance and subsea productivity: closing the loop with connectivity and measurements. In SPE Annual Technical Conference and Exhibition. OnePetro.

Rogel, E., Leon, O., Espidel, Y., Gonzalez, Y., 2001. Asphaltene stability in crude oils. SPE Prod. Facil. 16 (02), 84–88.

Rogel, E., Leon, O., Torres, G., & Espidel, J. (2000). Aggregation of asphaltenes in organic solvents using surface tension measurements. Fuel, 79(11), 1389-1394.

Rudrake, A., Karan, K., & Horton, J. H. (2009). A combined QCM and XPS investigation of asphaltene adsorption on metal surfaces. Journal of colloid and interface science, 332(1), 22-31.

S. Hassanpour, M.R. Malayeri, M. Riazi, Asphaltene Precipitation during Injection of CO2 Gas into a Synthetic Oil in the Presence of Fe3O4 and TiO2 Nanoparticles, J. Chem. Eng. Data 63 (5) (2018) 1266–1274

Saraji, S., Goual, L., & Piri, M. (2010). Adsorption of asphaltenes in porous media under flow conditions. Energy & fuels, 24(11), 6009-6017.

Scott, D. E., Schulze, M., Stryker, J. M., & Tykwinski, R. R. (2021). Deciphering structure and aggregation in asphaltenes: hypothesis-driven design and development of synthetic model compounds. Chemical Society Reviews, 50(16), 9202-9239.

Shojaati, F., Riazi, M., Mousavi, S. H., & Derikvand, Z. (2017). Experimental investigation of the inhibitory behavior of metal oxides nanoparticles on asphaltene precipitation. Colloids and Surfaces A: Physicochemical and Engineering Aspects, 531, 99-110.

Sisco, C., Abutaqiya, M. I. L., Wang, F., Zhang, J., Tavakkoli, M., & Vargas, F. M. (2018). Asphaltene Precipitation Modeling. In Asphaltene Deposition (pp. 111-159). CRC Press.

Smith, D. F., Klein, G. C., Yen, A. T., Squicciarini, M. P., Rodgers, R. P., & Marshall, A. G. (2008). Crude oil polar chemical composition derived from FT− ICR mass spectrometry accounts for asphaltene inhibitor specificity. Energy & Fuels, 22(5), 3112-3117.

Soler, C. A. C., Malagueta, D. C., & Martin, C. A. G. (2023). Feasibility of implementation of solar thermal energy in steam-assisted gravity drainage (SAGD) in extra-heavy oil field in Colombia. Geoenergy Science and Engineering, 222, 211463.

Soleymanzadeh, A., Yousefi, M., Kord, S., & Mohammadzadeh, O. (2019). A review on methods of determining onset of asphaltene precipitation. Journal of Petroleum Exploration and Production Technology, 9, 1375-1396.

Soroush, M., Roostaei, M., Hosseini, S. A., Mohammadtabar, M., Pourafshary, P., Mahmoudi, M., ... & Fattahpour, V. (2021). Challenges and potentials for sand and flow control and management in the sandstone oil fields of Kazakhstan: A literature review. SPE Drilling & Completion, 36(01), 208-231.

Speight, J. G. (2006). The Chemistry and Technology of Petroleum. 4th.

Sullivan, M., Smythe, E. J., Fukagawa, S., Harrison, C., Dumont, H., & Borman, C. (2020). A fast measurement of asphaltene onset pressure. SPE Reservoir Evaluation & Engineering, 23(03), 0962-0978.

Sun, J., Xu, Z., Li, W., & Shen, X. (2017). Effect of nano-SiO2 on the early hydration of alite-sulphoaluminate cement. Nanomaterials, 7(5), 102.

Tarboush, B. J. A., & Husein, M. M. (2012). Oxidation of asphaltenes adsorbed onto NiO nanoparticles. Applied Catalysis A: General, 445, 166-171.

Tavakkoli, M., He, P., Lin, P. H., Rezaee, S., Puerto, M., Doherty, R., ... & Vargas, F. M. (2017, May). Asphaltene deposition and fouling in reservoirs. In Offshore Technology Conference (p. D021S024R002). OTC.

Tavakkoli, M., Panuganti, S. R., Taghikhani, V., Pishvaie, M. R., & Chapman, W. G. (2014). Precipitated asphaltene amount at high-pressure and high-temperature conditions. Energy & fuels, 28(3), 1596-1610.

Thakur, S., Pandey, S., & Arotiba, O. A. (2016). Development of a sodium alginate-based organic/inorganic superabsorbent composite hydrogel for adsorption of methylene blue. Carbohydrate polymers, 153, 34-46.

Thakur, S., Pandey, S., & Arotiba, O. A. (2017). Sol-gel derived xanthan gum/silica nanocomposite—a highly efficient cationic dyes adsorbent in aqueous system. International journal of biological macromolecules, 103, 596-604.

Thommes, M., Kaneko, K., Neimark, A. V., Olivier, J. P., Rodriguez-Reinoso, F., Rouquerol, J., & Sing, K. S. (2015). Physisorption of gases, with special reference to the evaluation of surface area and pore size distribution (IUPAC Technical Report). Pure and applied chemistry, 87(9-10), 1051-1069.

Wang, T., Zhong, X., Zhang, Z., Yuan, X., Zhou, L., Zheng, Z., ... & Hu, J. (2022). Asphaltene adsorption of Co3O4 nanoparticles modified by SiO2 film. Applied Surface Science, 602, 154267.

Xing, C., Hilts, R. W., & Shaw, J. M. (2010). Sorption of Athabasca vacuum residue constituents on synthetic mineral and process equipment surfaces from mixtures with pentane. Energy & Fuels, 24(4), 2500-2513.

Y. Kazemzadeh, M.R. Malayeri, M. Riazi, R. Parsaei, Impact of Fe3O4 nanoparticles on asphaltene precipitation during CO2 injection, J. Nat. Gas Sci. Eng. 22 (2015) 227–234

Zhao, J., & Liu, X. (2022). Electron microscopic methods (TEM, SEM and energy dispersal spectroscopy).